Dynamics of non-Abelian strings in the theory interpolating from $\mathcal{N}=2$ to $\mathcal{N}=1$ supersymmetric QCD

A. Gorsky,[1,2] E. Ievlev,[3,4,*] and A. Yung[3,5]

[1]*Institute for Information Transmission Problems of RAS, Moscow, Russia*
[2]*Moscow Institute of Physics and Technology, Dolgoprudnyi, Russia*
[3]*National Research Center "Kurchatov Institute," Petersburg Nuclear Physics Institute, Gatchina, St. Petersburg 188300, Russia*
[4]*St. Petersburg State University, Universitetskaya nab., St. Petersburg 199034, Russia*
[5]*William I. Fine Theoretical Physics Institute, University of Minnesota, Minneapolis, Minnesota 55455, USA*

(Received 26 November 2019; published 21 January 2020)

We study the dynamics of non-Abelian vortex strings supported in $\mathcal{N}=2$ supersymmetric QCD with the U(N) gauge group and $N_f=N$ quark flavors deformed by the mass μ of the adjoint matter. In the limit of large μ the bulk four-dimensional theory flows to $\mathcal{N}=1$ supersymmetric QCD. The dynamics of orientational zero modes of the non-Abelian string is described by the world sheet $CP(N-1)$ model. At $\mu=0$ this model has $\mathcal{N}=(2,2)$ supersymmetry while at large μ it flows to the nonsupersymmetric $CP(N-1)$ model. We solve the world sheet model in the large N approximation and find a rich phase structure with respect to the deformation parameter μ and quark mass differences. The phases include two strong coupling phases and two Higgs phases. In particular, the Higgs phase at small μ supports $CP(N-1)$ model kinks representing confined monopoles of the bulk QCD, while in the large-μ Higgs phase monopoles disappear.

DOI: 10.1103/PhysRevD.101.014013

I. INTRODUCTION

Non-Abelian vortex strings were first found in $\mathcal{N}=2$ supersymmetric QCD (SQCD) with gauge group U(N) and $N_f=N$ flavors of quark hypermultiplets [1–4]; see [5–8] for reviews. When this theory is in the Higgs phase for scalar quarks (in the quark vacuum), non-Abelian strings are formed. They give rise to the confinement of monopoles at weak coupling and to the so-called "instead-of-confinement" phase for quarks at strong coupling; see [9] for a review. This picture gives a non-Abelian generalization of the Seiberg-Witten scenario of the Abelian quark confinement in the monopole vacuum of $\mathcal{N}=2$ SQCD [10,11].

Besides translational zero modes typical for Abrikosov-Nielsen-Olesen (ANO) strings [12] non-Abelian strings have orientational zero modes. Their internal dynamics is described by the two-dimensional $\mathcal{N}=(2,2)$ supersymmetric $CP(N-1)$ model living on the string world sheet [1–4].

A lot of work has been done to generalize the construction of non-Abelian strings to QCD-like theories with less supersymmetry, in particular to $\mathcal{N}=1$ SQCD [13–16]; see [7] for a review. One promising approach is to deform $\mathcal{N}=2$ SQCD by the mass μ of the adjoint matter (μ-deformed SQCD) and study what happens to non-Abelian strings upon this deformation. This deformation breaks $\mathcal{N}=2$ supersymmetry, and in the limit of $\mu\to\infty$ the bulk theory flows to $\mathcal{N}=1$ SQCD. In Ref. [16] the world sheet theory living on the non-Abelian string in the μ-deformed SQCD was found, and it was shown that it flows to the nonsupersymmetric $CP(N-1)$ model in the limit of large μ.

Since the bulk SQCD is in the Higgs phase for scalar quarks, monopoles are confined by non-Abelian strings. However, the monopoles cannot be attached to the string end points. In fact, in the U(N) theories confined monopoles are junctions of two distinct elementary non-Abelian strings. From the point of view of the $CP(N-1)$ model living on the string world sheet, confined monopoles are seen as kinks interpolating between different vacua of the $CP(N-1)$ model [3,4,17] (see [7] for a review).

In this paper we present a large N solution of the world sheet theory for the non-Abelian string in the μ-deformed

*Corresponding author.
ievlevea@thd.pnpi.spb.ru

SQCD. The large N approximation was first used by Witten to solve both nonsupersymmetric and $\mathcal{N}=(2,2)$ supersymmetric two-dimensional $CP(N-1)$ models [18]. In particular, the large-N Witten's solution shows that an auxiliary U(1) gauge field A_μ introduced to formulate the $CP(N-1)$ model becomes physical. The $\mathcal{N}=(2,2)$ supersymmetric $CP(N-1)$ model has N degenerate vacua as dictated by its Witten index. The order parameter which distinguishes between these vacua is the vacuum expectation value (VEV) of the scalar superpartner σ of the gauge field A_μ [18].

In the nonsupersymmetric $CP(N-1)$ model these vacua are split with splittings proportional to $1/N$ and become quasivacua. The theory has a single true vacuum.[1] The order parameter that distinguishes between these quasivacua is the value of the constant field strength of the gauge field A_μ which is massless in the nonsupersymmetric case [18]; see also [19] and review [7].

In this paper we use the large N approximation to study a phase structure of the world sheet theory on the non-Abelian string in μ-deformed SQCD with respect to the deformation parameter μ and quark mass differences Δm. We find a rich phase structure which includes two strong coupling phases and two Higgs phases.

Strong coupling phases appear at small Δm. The first strong coupling phase appears at small μ. It is qualitatively similar to the $\mathcal{N}=(2,2)$ supersymmetric phase at $\mu=0$. Although N vacua are split and become quasivacua, the order parameter is still the VEV of the field σ. In the second strong coupling phase at large μ quasivacua are distinguished by the value of the constant electric field. This phase is qualitatively similar to the nonsupersymmetric $CP(N-1)$ model.

At large Δm we find two weakly coupled Higgs phases. At small μ, N vacua present in the $\mathcal{N}=(2,2)$ case split and become quasivacua. Still we have kinks interpolating between them. As we increase μ above a certain critical value, these lifted quasivacua disappear one by one, so we have a cascade of phase transitions. In the end we are left with a single vacuum and no kinks at all.

From the point of view of the bulk SQCD we interpret this as follows. At large Δm and small μ we have monopoles confined by non-Abelian strings while as we increase μ monopoles disappear.

The paper is organized as follows. In Sec. II we review nonsupersymmetric and $\mathcal{N}=(2,2)$ supersymmetric $CP(N-1)$ models and their large-N solutions. We also formulate the world sheet $CP(N-1)$ model for non-Abelian string in μ-deformed SQCD. In Sec. III we derive the effective potential of this model in the large N approximation. Section IV is devoted to the discussion of the two strong coupling phases at small Δm, while in Sec. V we study Higgs phases at large Δm. In Sec. VI we make brief comments on the brane picture of non-Abelian strings and 2d-4d correspondence, i.e., a map between certain quantities in the bulk and world sheet theories. Section VII contains the description of the phase diagram of the world sheet model and our conclusions.

[1]We assume below that the θ angle is zero.

II. REVIEW OF $CP(N-1)$ SIGMA MODELS

In this section we define basic $CP(N-1)$ models that are of interest to us. First, we will briefly review the nonsupersymmetric and the $\mathcal{N}=(2,2)$ supersymmetric models, which were considered before; see, for example, [18,20–22]. After that, we will introduce the model that we will be working with, namely the μ-deformed $CP(N-1)$ model which is an effective theory living on the world sheet of non-Abelian string in μ-deformed SQCD [16].

A. Nonsupersymmetric model

Throughout this paper we will be working with the gauge formulation [18] of the $CP(N-1)$ models. In this formalism, the model is formulated via N complex scalar fields n^i, $i=1,\ldots,N$, interacting with auxiliary U(1) gauge field A_μ. The Lagrangian is written as

$$\mathcal{L}=|\nabla_\mu n^i|^2+iD(\bar{n}_i n^i-2\beta_0)+\sum_i|\sqrt{2}\sigma-m_i|^2|n^i|^2, \quad (2.1)$$

where $\nabla_\mu=\partial_\mu-iA_\mu$. Fields σ and D come without kinetic energy and are also auxiliary. They can be eliminated via their equations of motion. In particular, integrating out D imposes the constraint

$$\bar{n}_i n^i=2\beta_0, \quad (2.2)$$

which together with gauge invariance reduces the number of real degrees of freedom (d.o.f.) of the n^i field down to $2(N-1)$.

This is the nonsupersymmetric version of the $CP(N-1)$ model, and it arises as a world sheet theory on the non-Abelian string in a nonsupersymmetric QCD-like theory; see [19] and review [7]. The mass parameters m_i are equal to quark masses in the four-dimensional theory.

Throughout this paper we will consider the masses placed uniformly on a circle,

$$m_k=m-\Delta m\exp\left(\frac{2\pi ik}{N}\right), \qquad k=0,\ldots,N-1. \quad (2.3)$$

Here $m\in\mathbb{R}$ is the average mass, and $\Delta m>0$ is effectively the mass scale of the model. Note that by a shift of σ one can always add a constant to all m_i. In particular, one can get rid of the average mass m.

The bare coupling constant β_0 in quantum theory becomes a running coupling β. It is asymptotically free and defines the scale Λ_{CP} via

$$\Lambda_{CP}^2 = M_{\rm uv}^2 \exp\left(-\frac{8\pi\beta_0}{N}\right), \tag{2.4}$$

where $M_{\rm uv}$ is the ultraviolet (UV) cutoff.

Let us review phases of this theory. It is known that in the case of vanishing masses $\Delta m = 0$ this nonsupersymmetric $CP(N-1)$ model is at strong coupling with vanishing VEV $\langle n^i \rangle = 0$. It can be solved by means of the $1/N$ expansion [18]. It turns out that at the quantum level spontaneous breaking of the global SU(N) (flavor) symmetry present at the classical level disappears. There are no massless Goldstone bosons in the physical spectrum. The n^i fields acquire mass of the order of Λ_{CP}.

Moreover, a composite d.o.f.—the would-be auxiliary photon A_μ—acquires a kinetic term at the one-loop level and becomes dynamical. The presence of a massless photon ensures long range forces in the nonsupersymmetric $CP(N-1)$ model. The Coulomb potential is linear in two dimensions, namely

$$V(r) \sim \frac{\Lambda_{CP}^2}{N} r, \tag{2.5}$$

where r is the separation between the charges. This leads to the Coulomb/confinement phase [18]. Electric charges are confined. The lightest electric charges are the n^i quanta which become kinks at strong coupling [18]. The confinement of kinks means that they are not present in the physical spectrum of the theory in isolation. They form bound states, kink-antikink "mesons."

Masses of kinks are of order of Λ_{CP} while the confining potential is weak, proportional to $1/N$. Therefore kink and antikink in the meson are well separated forming a quasivacuum inside the meson. Thus, beside the single ground state, there is a family of quasivacua with energy splittings of order $\sim\Lambda_{CP}^2/N$. The order parameter which distinguishes different quasivacua is the value of the constant electric field or topological density

$$Q = \frac{i}{2\pi}\varepsilon_{\mu\nu}\partial^\mu A^\nu = \frac{1}{8\pi\beta}\varepsilon_{\mu\nu}\partial^\mu \bar{n}_i \partial^\nu n^i. \tag{2.6}$$

The picture of confinement of n's is shown on Fig. 1.

The kinks interpolate between the adjacent vacua. They are confined monopoles of the bulk theory. Since the excited string tensions are larger than the tension of the lightest one, these monopoles, besides four-dimensional confinement, are confined also in the two-dimensional sense: a monopole is necessarily attached to an antimonopole on the string to form a mesonlike configuration [19,23].

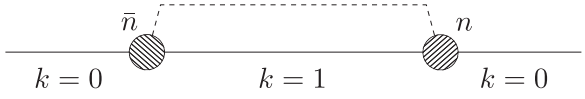

FIG. 1. Linear confinement of the n-$\bar{n}$ pair. The solid straight line represents the ground state ($k=0$ vacuum). The dashed line shows the vacuum energy density in the first quasivacuum.

On the other hand, at large mass scales $\Delta m \gg \Lambda_{CP}$ the coupling constant is small, frozen at the scale Δm, and semiclassical calculations are applicable. The field n^i develops a nonzero VEV, and there is no massless photon and no long-range interactions. That is why this phase is usually called the "Higgs phase" as opposed to the Coulomb/confinement strong coupling phase. More exactly the $CP(N-1)$ model in this phase gives a low energy description of a Higgs phase below the scale of the photon mass. Essentially this weakly coupling Higgs phase is similar to the "classical phase" described by the classical Lagrangian (2.1).

It was shown that at intermediate mass scales $\Delta m \sim \Lambda_{CP}$ there is a phase transition between the Higgs and Coulomb phases; see [19,21,24,25].

B. $\mathcal{N}=(2,2)$ model

Supersymmetric generalization of the above model [18,20] has additional fermionic field ξ^i, $i=1,\ldots,N$, which are superpartners of the n_i fields. The Euclidean version of the full $\mathcal{N}=(2,2)$ Lagrangian is

$$\begin{aligned}\mathcal{L} = {}& \frac{1}{e_0^2}\left(\frac{1}{4}F_{\mu\nu}^2 + |\partial_\mu\sigma|^2 + \frac{1}{2}D^2 + \bar{\lambda} i\bar{\sigma}^\mu\partial_\mu\lambda\right) + iD(\bar{n}_i n^i - 2\beta_0) \\ & + |\nabla_\mu n^i|^2 + \bar{\xi}_i i\bar{\sigma}^\mu\nabla_\mu\xi^i + 2\sum_i\left|\sigma - \frac{m_i}{\sqrt{2}}\right|^2 |n^i|^2 \\ & + i\sqrt{2}\sum_i\left(\sigma - \frac{m_i}{\sqrt{2}}\right)\bar{\xi}_{Ri}\xi_L^i - i\sqrt{2}\bar{n}_i(\lambda_R\xi_L^i - \lambda_L\xi_R^i) \\ & + i\sqrt{2}\sum_i\left(\bar{\sigma} - \frac{\bar{m}_i}{\sqrt{2}}\right)\bar{\xi}_{Li}\xi_R^i - i\sqrt{2}n^i(\bar{\lambda}_L\bar{\xi}_{Ri} - \bar{\lambda}_R\bar{\xi}_{Li}),\end{aligned} \tag{2.7}$$

where m_i are twisted masses and the limit $e_0^2 \to \infty$ is implied. Moreover, $\bar{\sigma}^\mu = \{1, i\sigma_3\}$. Fermions ξ_L and ξ_R are, respectively, left and right components of the ξ field. Here again one can add a uniform constant to all the m_i by shifting the σ field.

The gauge field A_μ, complex scalar superpartner σ, real scalar D, and a two-component complex fermion λ form a vector auxiliary supermultiplet. In particular, integrating over D and fermion λ give the constraints

$$\bar{n}_i n^i = 2\beta_0, \tag{2.8}$$

$$\bar{n}_i\xi^i = 0, \qquad \bar{\xi}_i n^i = 0 \tag{2.9}$$

in the limit $e_0 \to \infty$.

This model was derived as a world sheet theory on the non-Abelian string in $\mathcal{N}=2$ SQCD. The n_i fields

parametrize the orientational moduli of the non-Abelian string [1–4]. The mass parameters m_i are in fact masses of the bulk quark fields. The bare coupling constant β_0 is related to the bulk gauge coupling constant g^2 normalized at the scale of the bulk gauge boson mass $m_G \sim g\sqrt{\mu m}$ via (see e.g., [7])

$$2\beta_0 = \frac{4\pi}{g^2(m_G)} = \frac{N}{2\pi}\ln\frac{m_G}{\Lambda_{CP}}. \tag{2.10}$$

In order to keep the bulk theory at weak coupling we assume that $m_G \gg \Lambda_{CP}$.

Witten solved this model in the large N approximation in the zero mass case [18]. The large-N solution of this model at nonzero masses shows two different regimes at weak and strong couplings [26]. At small mass scales $\Delta m < \Lambda_{CP}$ the theory is in the strong coupling phase with zero VEV $\langle n^i \rangle = 0$ and with a dynamical photon (Witten's phase). However, the photon now is massive due to the presence of the chiral anomaly. There are no long-range forces and no confinement of kinks.

In both strong and weak coupling regimes the theory has N degenerate vacuum states as dictated by its Witten index. They are labeled by the VEV of σ [26]. At $\Delta m < \Lambda_{CP}$ we have

$$\sqrt{2}\sigma = \exp\left(\frac{2\pi i k}{N}\right) \times \Lambda_{CP}, \qquad k = 0, \ldots, N-1. \tag{2.11}$$

This result can be understood as follows. The chiral anomaly breaks U(1) R-symmetry present at zero masses down to Z_{2N} which is then broken spontaneously down to Z_2 by VEV of the σ field (which has R charge equal to two). In particular, from the large-N solution it follows that VEV of $\sqrt{2}|\sigma| = \Lambda_{CP}$. Then Z_{2N} symmetry ensures the presence of N vacua as shown in Eq. (2.11).

At large masses located on a circle [see (2.3)] the Z_{2N} symmetry is still unbroken. This leads to the similar structure of the σ VEVs at $\Delta m > \Lambda_{CP}$, namely

$$\sqrt{2}\sigma = \exp\left(\frac{2\pi i k}{N}\right) \times \Delta m, \qquad k = 0, \ldots, N-1. \tag{2.12}$$

The above formulas show a phase transition at $\Delta m = \Lambda_{CP}$. As follows from the large-N solution the model above this point is in the Higgs phase with a nonzero VEV for, say, the zero component of n, $\langle n^0 \rangle \neq 0$. In both phases there is no confinement, in contrast to the nonsupersymmetric case.

In fact, the above phase transition is a consequence of the large-N approximation. At finite N the transition between two regimes is smooth. This follows from the exact effective superpotential known for the $\mathcal{N} = (2,2)$ $CP(N-1)$ model [20].

C. μ-Deformed $CP(N-1)$ model

Now let us pass on to the case of interest, namely, the μ-deformed $CP(N-1)$ model. This model appears as a world sheet theory on a non-Abelian string in $\mathcal{N} = 2$ SQCD deformed by the adjoint field mass μ. It was derived in [16] in two cases, for small and large values of the deformation μ. Here and throughout this paper we will take the mass parameters to lie on the circle (2.3), and we also assume that the deformation parameter is real and positive, $\mu > 0$.

The first effect derived in [16] is that n_i fields entering the $\mathcal{N} = (2,2)$ $CP(N-1)$ model (2.7) develop an additional potential upon μ deformation which depends on mass differences. This potential in the small μ limit was first found in [27]. The second effect is that superorientational modes of the non-Abelian string are lifted. In other words the two-dimensional fermions ξ^i (fermionic superpartners of n^i) were massless in the supersymmetric version of the model at $\mu = 0$. However, at small μ they acquire a mass $\lambda(\mu) \sim \mu$ [16]. At large deformations they become heavy and decouple.

In order to capture these features, we write the following Lagrangian for the deformed $CP(N-1)$ model:

$$\begin{aligned}\mathcal{L} = {} & |\nabla_\mu n^i|^2 + \bar{\xi}_i i\bar{\sigma}^\mu \nabla_\mu \xi^i + iD(\bar{n}_i n^i - 2\beta) \\ & + \sum_i |\sqrt{2}\sigma - m_i|^2 |n^i|^2 + v(\mu)\sum_i \Re\Delta m_{i0}|n^i|^2 \\ & + i\sum_i (\sqrt{2}\sigma - m_i - \lambda(\mu))\bar{\xi}_{Ri}\xi^i_L - i\sqrt{2}\bar{n}_i(\lambda_R \xi^i_L - \lambda_L \xi^i_R) \\ & + i\sum_i (\sqrt{2}\bar{\sigma} - \bar{m}_i - \lambda(\bar{\mu}))\bar{\xi}_{Li}\xi^i_R - i\sqrt{2}n^i(\bar{\lambda}_L \bar{\xi}_{Ri} - \bar{\lambda}_R \bar{\xi}_{Li}),\end{aligned} \tag{2.13}$$

where $\Delta m_{i0} = m_i - m_0$, m_i are quark masses $i = 1, \ldots, N$, and m_0 is the mass with the smallest real part.

The coefficient functions $v(\mu)$ and $\lambda(\mu)$ were derived in [16] at the classical level for small and large values of μ:

$$v(\mu) = \begin{cases} \frac{4\pi\mu}{2\beta}, & \mu \to 0, \\ \frac{1}{2\beta}\frac{8\pi\mu}{\ln\frac{a^2\mu}{m}}, & \mu \to \infty, \end{cases} \tag{2.14}$$

$$\lambda(\mu) = \begin{cases} \lambda_0 \frac{\mu}{2\beta}, & \mu \to 0, \\ \text{const } g\sqrt{\mu m} \sim m_G, & \mu \to \infty. \end{cases} \tag{2.15}$$

Here g^2 is the four-dimensional bulk coupling constant. The numerical value for λ_0 is $\lambda_0 \approx 3.7$ [16]. Note that although we can get rid of the explicit dependence on the average quark mass m in (2.13) by a shift of σ, the above formulas show that it enters indirectly through definitions of parameters of μ-deformed $CP(N-1)$ model (2.13) in terms of parameters of the bulk SQCD.

This model interpolates between the supersymmetric and the nonsupersymmetric models briefly described above. In the limit $\mu \to 0$ supersymmetry is restored to $\mathcal{N} = (2,2)$, and we obtain (2.7). At large deformations the fermions can be integrated out, and the theory flows to the bosonic model (2.1).

Our main tool for investigating this model in the quantum level will be the $1/N$ expansion. In order to have a smooth large N limit, our parameters should scale as

$$g^2 \sim 1/N, \qquad \beta \sim N, \qquad \mu \sim N,$$
$$m \sim 1, \qquad v(\mu) \sim 1, \qquad \lambda(\mu) \sim 1. \tag{2.16}$$

Below in this paper we will use three independent physical parameters to describe our four-dimensional bulk model. The first one is the bulk gauge boson mass

$$m_G^2 = 2g^2\mu m, \tag{2.17}$$

which plays a role of the physical UV cutoff in the world sheet $CP(N-1)$ model on the non-Abelian string; see [7]. The second one is the quark mass differences $(m_i - m_j)$, and the third parameter is the physical mass of the adjoint matter

$$m_{\rm adj} = g^2\mu = \frac{\mu}{\frac{N}{8\pi^2}\ln\frac{m_G}{\Lambda_{4d}}} \equiv \tilde{\mu}, \tag{2.18}$$

which will be our actual deformation parameter. All three parameters scale as N^0 in the large N limit. Here Λ_{4d} is the scale of the $\mathcal{N} = 2$ bulk SQCD.

Thus, in fact, the average quark mass m is not an independent parameter. It can be written as

$$m = \frac{m_G^2}{2\tilde{\mu}}. \tag{2.19}$$

At the scale of the gauge boson mass (2.17) the world sheet coupling constant for small μ is given by [2,3] [cf. (2.10)]

$$2\beta = \frac{4\pi}{g^2} = \frac{N}{2\pi}\ln\frac{m_G}{\Lambda_{4d}}. \tag{2.20}$$

For large μ the world sheet coupling normalized at the scale m_G becomes [16]

$$2\beta = \text{const}\frac{\mu}{m}\frac{1}{\ln^2\frac{g^2\mu}{m}}. \tag{2.21}$$

Expressed in terms of the invariant parameters it reads

$$2\beta = \text{const}\frac{N}{\pi}\frac{\tilde{\mu}^2}{m_G^2}\frac{\ln\frac{m_G}{\Lambda_{4d}^{\mathcal{N}=1}}}{\ln^2\frac{2\tilde{\mu}}{m_G}}, \tag{2.22}$$

where we take into account that at large $\tilde{\mu}$ our bulk theory flows to $\mathcal{N} = 1$ SQCD with the scale $(\Lambda_{4d}^{\mathcal{N}=1})^{2N} = \tilde{\mu}^N\Lambda_{4d}^N$.

In terms of the independent parameters the coefficient functions v and λ become

$$v(\tilde{\mu}) = \begin{cases} \tilde{\mu}, & \tilde{\mu} \to 0, \\ \frac{m_G^2}{\tilde{\mu}}\ln\frac{2\tilde{\mu}}{m_G}, & \mu \to \infty, \end{cases} \tag{2.23}$$

$$\lambda(\tilde{\mu}) = \begin{cases} \tilde{\lambda}_0\tilde{\mu}, & \tilde{\mu} \to 0, \\ m_G, & \tilde{\mu} \to \infty, \end{cases} \tag{2.24}$$

where $\tilde{\lambda}_0 = \lambda_0/4\pi \approx 0.3$.

As we already mentioned, the value of the bulk gauge boson mass m_G plays a role of the UV cutoff of our world sheet theory. Below m_G our model is asymptotically free [cf. (2.4)] with

$$2\beta(E) = \frac{N}{2\pi}\ln\frac{E}{\Lambda_{2d}} \tag{2.25}$$

at the scale E. This fixes the scale Λ_{2d} in terms of the parameters of the bulk theory. At small $\tilde{\mu}$ we have

$$\Lambda_{2d}(\tilde{\mu} \to 0) = \Lambda_{4d}, \tag{2.26}$$

while at large $\tilde{\mu}$

$$\Lambda_{2d} = \Lambda_{4d}^{\mathcal{N}=1}\exp\left(-\text{const}\frac{\tilde{\mu}^2}{m_G^2}\cdot\frac{1}{\ln\frac{2\tilde{\mu}}{m_G}}\right). \tag{2.27}$$

Note that at $\tilde{\mu} \to \infty$ the scale (2.27) of our model becomes exponentially small and the model enters the strong coupling regime only at extremely small energies. We will see below that phase transitions with respect to $\tilde{\mu}$ appear at rather small values of $\tilde{\mu}$ where the scale Λ_{2d} is close to its supersymmetric value Λ_{4d}. Since the fermion decoupling occurs at very large $\tilde{\mu} \gg m_G$, we can use small $\tilde{\mu}$ approximation formulas (2.23) and (2.24) while investigating the phase transition.

In the following sections we are going to investigate different phases and vacuum structure of the world sheet theory. There are two parameters that we can vary—the SUSY breaking parameter $\tilde{\mu}$ and the mass scale Δm. As we already mentioned, our model (2.13) exhibits a rich phase structure in the $(\Delta m, \tilde{\mu})$ plane.

III. ONE-LOOP EFFECTIVE POTENTIAL

In this section we proceed with solving the theory (2.13) via the $1/N$ expansion. As we already mentioned, the $\mathcal{N} = (2,2)$ model as well as the nonsupersymmetric $CP(N-1)$ model (without mass parameters) was solved by Witten [18]. This method was also generalized for the case of the heterotic $\mathcal{N} = (0,2)$ model [28] and for the twisted mass case [21,26]. Our derivation will closely follow these papers.

A. Derivation of the effective potential

We want to start by deriving the one-loop effective potential. Our action (2.13) is well suited for that since it is quadratic with respect to the dynamical fields n_i and ξ_i. However, we do not integrate over all of them *a priori* due to the following reason.

As was stated in the previous section, our model (2.13) is, in a sense, an intermediate case between the $\mathcal{N}=(2,2)$ and the nonsupersymmetric $CP(N-1)$ models, which were studied before. Therefore we can use the insights derived from these models in order to better understand our case. First of all, we expect that our theory has at least two phases, the strong and weak couplings. The order parameter distinguishing between these two phases is the expectation value of the n_i fields. At the weak coupling (the so-called Higgs phase [21]) one of the n_i develops a VEV, $\langle n_{i_0}\rangle = 2\beta$. In the strong coupling regime (the so-called Coulomb phase), VEVs of all the n_i fields vanish.

So, we will use the following strategy. We integrate over $N-1$ fields n^i with $i \neq 0$ (and over the corresponding fermions ξ_i). The resulting effective action is a functional of $n^0 \equiv n$, D, and σ. To find the vacuum configuration, we will minimize the effective action with respect to n, D, and σ.

Note that this functional also depends on A_μ and the fermions $\xi^0_{L,R}$ and $\lambda_{L,R}$, but the Lorenz invariance implies that these fields have zero VEVs. We also choose to allow n^0 field to have a nonzero VEV because the associated mass m_0 has the minimal real part [see (2.3)] and as we will see later $\langle n^0\rangle \neq 0$ corresponds to the true vacuum in the Higgs phase rather then a quasivacuum.

Integrating out the n^i and ξ^i fields, we arrive at the following determinants:

$$\frac{\prod_{i=1}^{N-1}\det(-\partial_k^2+|\sqrt{2}\sigma-m_i-\lambda(\mu)|^2)}{\prod_{i=1}^{N-1}\det(-\partial_k^2+iD+v(\mu)\Delta m_{i0}+|\sqrt{2}\sigma-m_i|^2)}, \tag{3.1}$$

which gives for the effective potential:

$$\begin{aligned} V_{\text{eff}} = &\int d^2x(iD+|\sqrt{2}\sigma-m_0|^2)|n|^2-2\beta\int d^2xiD \\ &+\sum_{i=1}^{N-1}\text{Tr}\,\ln(-\partial_k^2+iD+v(\mu)\Delta m_{i0}+|\sqrt{2}\sigma-m_i|^2) \\ &-\sum_{i=1}^{N-1}\text{Tr}\,\ln(-\partial_k^2+|\sqrt{2}\sigma-m_i-\lambda(\mu)|^2). \end{aligned} \tag{3.2}$$

The next step is to calculate the traces entering this expression. At $\tilde{\mu}\to 0$, the supersymmetry is restored, and this expression is well defined. However, at a nonvanishing deformation, this expression diverges quadratically, and a regularization needs to be performed. Below we proceed with the Pauli-Villars regularization (a similar procedure was carried out in [29]). We introduce regulator fields with masses b_a, f_a, $a=1,2$, and write the regularized effective potential as

$$\begin{aligned} V_{\text{eff}} = &\int d^2x(iD+|\sqrt{2}\sigma-m_0|^2)|n|^2-2\beta\int d^2xiD \\ &+\sum_{i=1}^{N-1}\text{Tr}\,\ln(-\partial_k^2+iD+v(\mu)\Delta m_{i0}+|\sqrt{2}\sigma-m_i|^2) \\ &+\sum_{a=1}^{2}\sum_{i=1}^{N-1}B_a\text{Tr}\,\ln(-\partial_k^2+b_a^2) \\ &-\sum_{i=1}^{N-1}\text{Tr}\,\ln(-\partial_k^2+|\sqrt{2}\sigma-m_i-\lambda(\mu)|^2) \\ &-\sum_{a=1}^{2}\sum_{i=1}^{N-1}F_a\text{Tr}\,\ln(-\partial_k^2+f_a^2), \end{aligned} \tag{3.3}$$

where the coefficients satisfy

$$\sum_{a=0}^{2}B_a=-1, \qquad \sum_{a=0}^{2}B_ab_a^2=-m_{\text{bos}}^2. \tag{3.4}$$

These equations imply

$$B_1=\frac{b_2^2-m_{\text{bos}}^2}{b_1^2-b_2^2}, \qquad B_2=-\frac{b_1^2-m_{\text{bos}}^2}{b_1^2-b_2^2}. \tag{3.5}$$

The regulator masses play the role of the UV cutoff. Similar relations hold for the fermionic regulator coefficients.

Moreover, we need to properly normalize our traces by subtracting the contributions in the trivial background, namely $\text{Tr}\,\ln(-\partial_k^2)$ from the bosonic and the fermionic traces. After this procedure we arrive at

$$\begin{aligned} V_{\text{eff}} = &\int d^2x(iD+|\sqrt{2}\sigma-m_0|^2)|n|^2-2\beta\int d^2xiD-\frac{1}{4\pi}\sum_{i=1}^{N-1}\Bigg[(+iD+v(\mu)\Delta m_{i0}+|\sqrt{2}\sigma-m_i|^2) \\ &\times\ln(+iD+v(\mu)\Delta m_{i0}+|\sqrt{2}\sigma-m_i|^2)-(+iD+v(\mu)\Delta m_{i0}+|\sqrt{2}\sigma-m_i|^2)\frac{b_1^2\ln b_1^2-b_2^2\ln b_2^2}{b_1^2-b_2^2}\Bigg] \\ &+\frac{1}{4\pi}\sum_{i=1}^{N-1}\Bigg[|\sqrt{2}\sigma-m_i-\lambda(\mu)|^2\ln|\sqrt{2}\sigma-m_i-\lambda(\mu)|^2-|\sqrt{2}\sigma-m_i-\lambda(\mu)|^2\frac{f_1^2\ln f_1^1-f_2^2\ln f_2^2}{f_1^2-f_2^2}\Bigg]. \end{aligned} \tag{3.6}$$

This is a quite complex expression. In order to simplify it, let us take the limit [29]

$$b_1^2=xM_{\text{uv}}^2, \qquad b_2^2=M_{\text{uv}}^2, \qquad f_1^2=xM_{\text{uv}}^2, \qquad f_2^2=M_{\text{uv}}^2, \qquad x\to 1, \tag{3.7}$$

where $M_{\rm uv}$ is the UV cutoff. Moreover, recall from Sec. II C that the bare coupling constant can be parametrized as

$$2\beta(M_{\rm uv}) = \frac{N}{4\pi}\ln\frac{M_{\rm uv}^2}{\Lambda^2}. \tag{3.8}$$

Here, $\Lambda \equiv \Lambda_{2d}$ is the scale of our model. Then the density of the effective potential becomes

$$\begin{aligned}\mathcal{V}_{\rm eff} = {} & (iD + |\sqrt{2}\sigma - m_0|^2)|n|^2 + \frac{1}{4\pi}\sum_{i=1}^{N-1} iD\left[1 - \ln\frac{iD + v(\mu)\Re\Delta m_{i0} + |\sqrt{2}\sigma - m_i|^2}{\Lambda^2}\right] \\ & + \frac{1}{4\pi}\sum_{i=1}^{N-1}(v(\mu)\Re\Delta m_{i0} + |\sqrt{2}\sigma - m_i|^2)\left[1 - \ln\frac{iD + v(\mu)\Re\Delta m_{i0} + |\sqrt{2}\sigma - m_i|^2}{M_{\rm uv}^2}\right] \\ & - \frac{1}{4\pi}\sum_{i=1}^{N-1}|\sqrt{2}\sigma - m_i - \lambda(\mu)|^2\left[1 - \ln\frac{|\sqrt{2}\sigma - m_i - \lambda(\mu)|^2}{M_{\rm uv}^2}\right].\end{aligned} \tag{3.9}$$

Note that our regularized effective potential depends on the UV cutoff scale $M_{\rm uv}$. We cannot make a subtraction to get rid of it in the model at hand for the following reason. First, when we consider our $\tilde{\mu}$-deformed $CP(N-1)$ model (2.13) as an effective world sheet theory on the non-Abelian string the UV cutoff has a clear physical meaning, namely

$$M_{\rm uv} = m_G, \tag{3.10}$$

where m_G is the mass of the bulk gauge boson. Moreover, the fermion mass $\lambda(\mu)$ in (3.9) interpolates from zero at $\tilde{\mu} = 0$ to $m_G = M_{\rm uv}$ at $\tilde{\mu} \to \infty$; see (2.24). Thus $M_{\rm uv}$ is in fact a physical parameter in our model, and there is no need to get rid of it.

The renormalized coupling constant is

$$2\beta_{\rm ren} = \frac{1}{4\pi}\sum_{i=1}^{N-1}\ln\frac{iD + v(\mu)\Re\Delta m_{i0} + |\sqrt{2}\sigma - m_i|^2}{\Lambda^2}. \tag{3.11}$$

B. Vacuum equations

To find the vacuum configuration we minimize the effective potential (3.9). Varying with respect to D we arrive at

$$|n|^2 = 2\beta_{\rm ren} = \frac{1}{4\pi}\sum_{i=1}^{N-1}\ln\frac{iD + v(\mu)\Re\Delta m_{i0} + |\sqrt{2}\sigma - m_i|^2}{\Lambda^2}. \tag{3.12}$$

Variation with respect to $\bar{n}$ yields the second equation:

$$(iD + |\sqrt{2}\sigma - m_0|^2)n = 0. \tag{3.13}$$

Finally, the third equation is obtained by minimizing over the σ field,

$$\begin{aligned}& -(\sqrt{2}\sigma - m_0)|n|^2 + \frac{1}{4\pi}\sum_{i=1}^{N-1}(\sqrt{2}\sigma - m_i) \\ & \quad\times \ln\frac{iD + v(\mu)\Re\Delta m_{i0} + |\sqrt{2}\sigma - m_i|^2}{m_G^2} \\ & = \frac{1}{4\pi}\sum_{i=1}^{N-1}(\sqrt{2}\sigma - m_i - \lambda(\mu))\ln\frac{|\sqrt{2}\sigma - m_i - \lambda(\mu)|^2}{m_G^2},\end{aligned} \tag{3.14}$$

where here and below we replaced $M_{\rm uv}$ by the physical mass m_G.

These three equations comprise our *master set*. In addition, the vacuum configurations must satisfy the constraint

$$\beta_{\rm ren} \geq 0, \tag{3.15}$$

which comes from $2\beta_{\rm ren} = |n|^2 \geq 0$.

From (3.12) and (3.13) it immediately follows that either

$$n = \beta_{\rm ren} = 0 \tag{3.16}$$

or

$$iD + |\sqrt{2}\sigma - m_0|^2 = 0. \tag{3.17}$$

The first option corresponds to the strong coupling regime where the VEV of n and the renormalized coupling constant vanish. The second option is realized in the Higgs regime, where the n field develops a VEV. In the following sections we will study each of these regimes in detail.

IV. STRONG COUPLING REGIME

In this section we will begin the investigation of our model in the strong coupling regime, which is defined by the condition (3.16). This phase occurs when the mass scale of the model $\Delta m \lesssim \Lambda$; see, e.g., [21,26]. To start off we will

first investigate a simple case $\Delta m = 0$. The behavior of our model is different at different values of the deformation parameter: at intermediate $\tilde{\mu}$ we will see a phase transition, while in the limit of large fermion mass $\lambda \to m_G$ we will confirm that the model (2.13) flows to the nonsupersymmetric $CP(N-1)$ model (2.1) as expected. Next, we will generalize our results to the case of distinct masses m_i.

A. Equal mass case, small deformations

We start by investigating the simplest case of equal mass parameters,

$$m_0 = m_1 = \cdots = m_{N-1} \equiv m. \tag{4.1}$$

Under this assumption the potential proportional to $v(\mu)$ is zero, and the only deformation we are left with is the fermion mass λ. For now we will not write its dependence on $\tilde{\mu}$ explicitly.

To simplify the equations, let us denote

$$\tau = \sqrt{2}\sigma - m_0. \tag{4.2}$$

Then the effective potential becomes

$$\mathcal{V}_{\text{eff}} = \frac{N}{4\pi} iD\left[1 - \ln\frac{iD + |\tau|^2}{\Lambda^2}\right] + \frac{N}{4\pi}|\tau|^2\left[1 - \ln\frac{iD + |\tau|^2}{m_G^2}\right] - \frac{N}{4\pi}|\tau - \lambda(\mu)|^2\left[1 - \ln\frac{|\tau - \lambda(\mu)|^2}{m_G^2}\right] + \Delta V(\arg\tau), \tag{4.3}$$

where $\tau = |\tau| e^{i \arg \tau}$. Here we added a new term $\Delta V(\arg\tau)$ absent in (3.9). It takes into account the chiral anomaly and appears already in the $\mathcal{N} = (2,2)$ $CP(N-1)$ model at $\tilde{\mu} = 0$. As was shown by Witten [18] the photon become massive due to the chiral anomaly with mass equal to 2Λ. The complex scalar σ is a superpartner of the photon and also acquires mass 2Λ. In particular, its argument $\arg\tau$ becomes massive.

This effect is taken into account by the additional potential $\Delta V(\arg\tau)$ in (4.3). It is constructed as follows. At small $\tilde{\mu}$ VEVs of τ are approximately given by their supersymmetric values,

$$\tau_k^{\text{SUSY}} = -\Lambda \exp\left(\frac{2\pi i k}{N}\right), \qquad k = 0, \ldots, N-1; \tag{4.4}$$

cf. (2.11). We divide 2π into N patches centered at vacuum values, $\arg\tau_k^{\text{SUSY}} = 2\pi k/N + \pi$, $k = 0, \ldots, (N-1)$, and define the potential $\Delta V(\arg\tau)$ to be quadratic in each patch. Namely, we have

$$\Delta V(\arg\tau) = \frac{N}{4\pi}\frac{m_{\arg\tau}^2}{2}(\arg\tau - \arg\tau_k^{\text{SUSY}})^2, \quad \frac{2\pi(k-\frac{1}{2})}{N} < \arg\tau - \pi < \frac{2\pi(k+\frac{1}{2})}{N}, \tag{4.5}$$

where $m_{\arg\tau}$ is the mass of $\arg\tau$. We present its calculation in Appendix A, in particular showing corrections [see Eq. (B7)] to Witten's result [18]

$$m_{\arg\tau}^{\text{SUSY}} = 2\Lambda. \tag{4.6}$$

Without the additional potential $\Delta V(\arg\tau)$ N discrete vacua (4.4) disappear immediately as we switch on $\tilde{\mu}$ due to the lifting of quasivacua. We show below that with $\Delta V(\arg\tau)$ taken into account quasivacua are still present at small $\tilde{\mu}$ and disappear only at certain finite critical $\tilde{\mu}_{\text{crit}}$ which we identify as a phase transition point. Note that possible higher corrections to the quadratic potential (4.5) are suppressed in the large N limit because the width of each patch is small, proportional to $1/N$.

1. Vacuum energies

As we turn on the deformation parameter $\tilde{\mu}$, the mass of the ξ^i fermion $\lambda(\tilde{\mu})$ is no longer zero. This breaks explicitly both chiral symmetry and two-dimensional supersymmetry. As a result the Z_N symmetry is broken and VEVs of σ are no longer located at a circle. Moreover, at $\tilde{\mu} = 0$ our model has N degenerate vacua given by (4.4). When we switch on $\tilde{\mu}$, the corresponding vacuum energies split, and all vacua except the one at $k = 0$ become quasivacua. The only true vacuum is the one at $k = 0$; see Fig. 2. As we discussed in Sec. II A, this leads to the confinement of kinks.

It turns out that there are two mechanisms responsible for the vacuum energy splitting. One is due to the effective potential (4.3) and dominates at small $\tilde{\mu}$. The other one is typical for the nonsupersymmetric $CP(N-1)$ model; see Sec. II A. It is due to the constant electric field of kinks interpolating between neighboring quasivacua and dominates at large $\tilde{\mu}$. We will now study the former mechanism, while the latter one will be considered in the next subsection.

Energy splittings in the small $\tilde{\mu}$ limit can be derived using the small $\lambda(\mu)$ expansion of the effective potential (4.3),

$$\mathcal{V}_{\text{eff}} = \mathcal{V}_{\text{SUSY}} + \delta\mathcal{V}, \tag{4.7}$$

where $\mathcal{V}_{\text{SUSY}}$ is the supersymmetric effective potential corresponding to $\lambda = 0$, while

$$\delta\mathcal{V} \approx \frac{N}{4\pi} \cdot 2\Re\tau \cdot \lambda \ln\frac{m_G^2}{|\tau|^2} \tag{4.8}$$

is the $O(\lambda)$ deformation. We can immediately infer lifted vacuum energies by plugging unperturbed VEVs (4.4) into (4.8). As we already mentioned, the ground state (true vacuum) is located at

$$\tau_0 = -\Lambda = \Lambda e^{i\pi}, \tag{4.9}$$

while the first quasivacuum is at

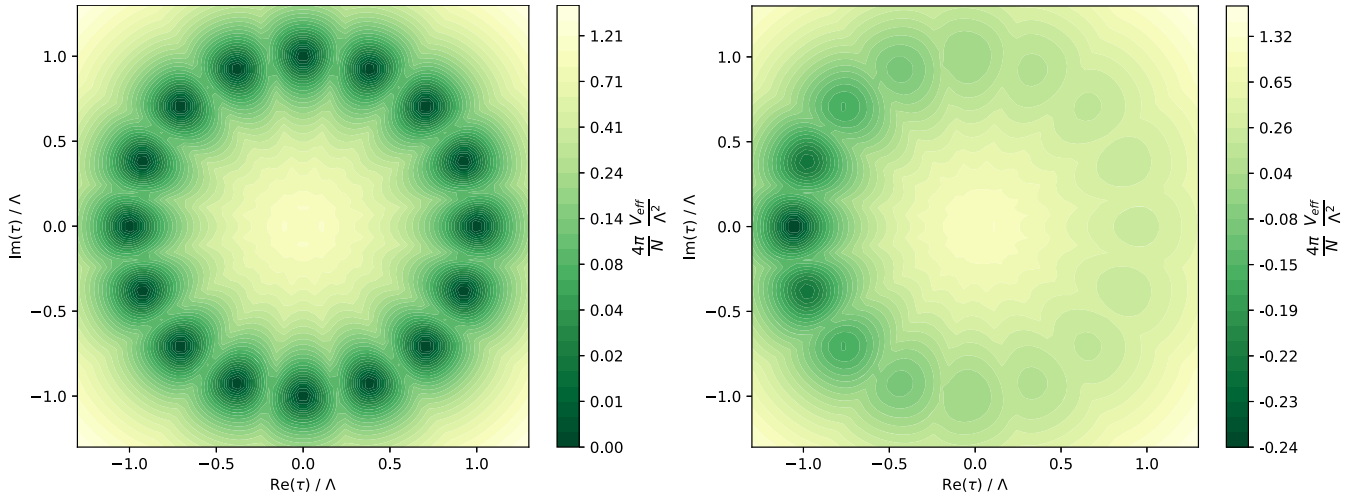

(a) $\lambda = 0$, supersymmetric case, degenerate vacua

(b) $\lambda > 0$, broken supersymmetry, lifted quasivacua

FIG. 2. Effective potential (4.3) on the complex $\tau = \sqrt{2}\sigma - m_0$ plane, with D integrated out.

$$\tau_1 = -\Lambda \exp\left(\frac{2\pi i}{N}\right) \approx -\Lambda - \Lambda\frac{2\pi i}{N} + \Lambda\frac{2\pi^2}{N^2}. \tag{4.10}$$

Plugging this into (4.8) we get for the vacuum splitting[2]

$$E_1 - E_0 = \frac{2\pi}{N}\lambda\Lambda \ln\frac{m_G}{\Lambda}. \tag{4.11}$$

This signifies that kinks interpolating between these vacua are now confined, as opposed to the supersymmetric case.

2. Corrections to the VEVs

Now let us derive corrections to the unperturbed VEVs (4.4). Minimizing the potential (4.3) we get

$$2\beta_{\text{ren}} = \ln\frac{iD + |\tau|^2}{\Lambda^2} = 0 \Rightarrow iD + |\tau|^2 = \Lambda^2, \tag{4.12}$$

$$|\tau| \ln\frac{|\tau - \lambda(\tilde{\mu})|^2}{\Lambda^2} + \cos(\arg\,\tau)\lambda(\tilde{\mu}) \ln\frac{m_G^2}{\Lambda^2} = 0, \tag{4.13}$$

$$-\sin(\arg\tau)\lambda|\tau|\ln\frac{m_G^2}{\Lambda^2} + \frac{m^2_{\arg\tau}}{2}(\arg\tau - \arg\tau_k^{\text{SUSY}}) = 0. \tag{4.14}$$

The approximate solution in the limit of small $\tilde{\mu}$ is given by

$$|\tau| \approx \Lambda - \cos(\arg\,\tau_k^{\text{SUSY}})\frac{1}{2}\lambda\ln\frac{m_G^2}{\Lambda^2}, \tag{4.15}$$

$$\arg\,\tau \approx \arg\,\tau_k^{\text{SUSY}} + \sin(\arg\,\tau_k^{\text{SUSY}})\frac{2\lambda\Lambda}{m^2_{\arg\,\tau}}\ln\frac{m_G^2}{\Lambda^2}. \tag{4.16}$$

[2]Formula (4.11) has a correction coming from the energy-momentum trace anomaly, but this correction is of the next order in the small parameter $\frac{\lambda}{\Lambda}\ln\frac{M_{\text{uv}}}{\Lambda}$.

In particular, for the $\tau_0 = -\Lambda$ we get the corrected value

$$\tau_{\text{ground}} \approx -\Lambda - \frac{1}{2}\lambda\ln\frac{m_G^2}{\Lambda^2}, \tag{4.17}$$

while for the first quasivacuum (4.10)

$$|\tau_1| \approx |\tau_{\text{ground}}| \approx \Lambda + \frac{1}{2}\lambda\ln\frac{m_G^2}{\Lambda^2},$$
$$\arg\,\tau_1 \approx \underbrace{\left(\pi + \frac{2\pi}{N}\right)}_{\text{unperturbed}} - \frac{2\pi}{N}\frac{\lambda}{2\Lambda}\ln\frac{m_G^2}{\Lambda^2}, \tag{4.18}$$

where we used (4.6) for the nonperturbed mass of σ. These results agree with numerical calculations; see Fig. 3.

Note that when

$$\frac{\lambda}{\Lambda}\ln\frac{m_G}{\Lambda} = 1, \tag{4.19}$$

we have in our approximation $\arg\,\tau_1 = \tau_{\text{ground}} = \pi$, and the quasivacuum at τ_1 effectively disappears. This signifies that around the point (4.19) a phase transition might take place. This will turn out to be true; see Sec. IV C below.

The quasivacuum with the highest energy is located at

$$\tau_{\text{high}} \approx \Lambda - \frac{1}{2}\lambda\ln\frac{m_G^2}{\Lambda^2}. \tag{4.20}$$

Further analysis of Eq. (4.13) shows that this solution disappears at

$$\lambda = \frac{2\Lambda}{e\ln\frac{m_G^2}{\Lambda^2}}, \tag{4.21}$$

which is consistent with (4.22). This suggests that around the critical value of the deformation

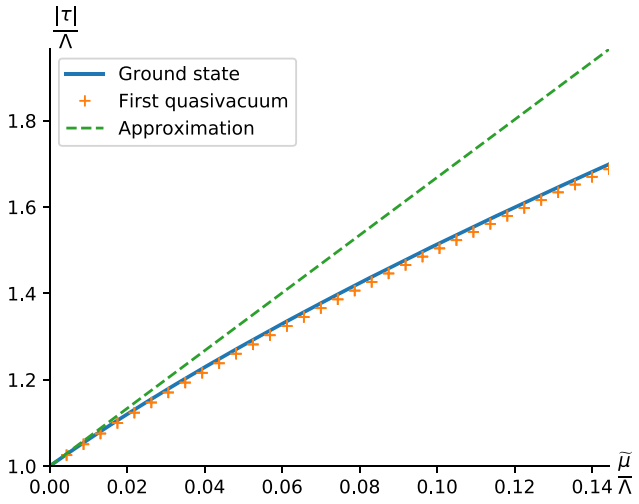

(a) $|\tau_{\text{ground}}|$ and $|\tau_1|$

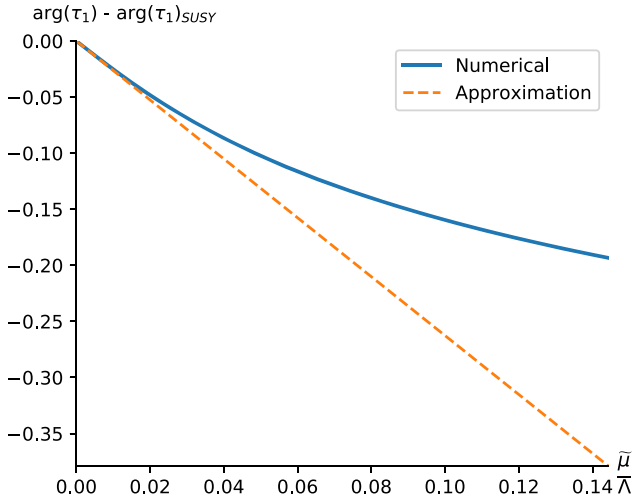

(b) Correction to arg τ_1

FIG. 3. Numerical results for the minima τ_{ground} and τ_1 obtained by directly minimizing (4.3). (a) The green dashed line shows the approximate formula (4.17), the solid blue line is the numerical values of $|\tau_{\text{ground}}|$, while $|\tau_1|$ is shown by red "+." (b) The approximate correction to arg τ_1 [(4.18), the last term] and the numerical results for this quantity.

$$\lambda_{\text{crit}} \sim \frac{\Lambda}{\ln \frac{m_G^2}{\Lambda^2}} \tag{4.22}$$

all quasivacua have decayed [cf. (4.19)].

B. Effective action

As we already mentioned, there are two mechanisms of the energy splitting of quasivacua at nonzero $\tilde{\mu}$. Both lead to the confinement of kinks. The first one is due to $\tilde{\mu}$ corrections present in the effective potential (4.3). These corrections lift σ quasivacua and lead to the splitting described by Eq. (4.11). The second mechanism is due to the constant electric field of kinks interpolating between quasivacua. The photon A_μ becomes dynamical on the quantum level [18]. We will see below that, as we turn on the deformation parameter $\tilde{\mu}$, the photon acquires a massless component. A linear Coulomb potential is generated, but the vacuum energy splitting due to the electrical field is much smaller than the one in (4.11). At sufficiently large $\tilde{\mu}$ all $N-1$ σ quasivacua decay, and the splitting is saturated by the electric field only. We identify this change of the regime and associated discontinuity in (the derivative of) $(E_1 - E_0)$ as a phase transition.

1. Derivation of the effective action

Consider now the effective action of our $\tilde{\mu}$-deformed $CP(N-1)$ model (2.13) obtained by integrating out n^i and ξ^i fields in the large-N approximation. Relaxing the condition that σ and D are constant fields assumed in Sec. III A we consider the one-loop effective action as a functional of fields of the vector supermultiplet.

Considering the vicinity of the true vacuum where $\Im\langle\sigma\rangle = 0$ we write down the bosonic part of the action in the form (Minkowski formulation[3])

$$S_{\text{eff}} = \int d^2x \Big\{ -\frac{1}{4e_\gamma^2} F_{\mu\nu}^2 + \frac{1}{e_{\Im\sigma}^2} |\partial_\mu \Im\sigma|^2 + \frac{1}{e_{\Re\sigma}^2} |\partial_\mu \Re\sigma|^2 - V(\sigma) - \sqrt{2} b_{\gamma,\Im\sigma} \Im\sigma F^* \Big\}, \tag{4.23}$$

where F^* is the dual gauge field strength,

$$F^* = -\frac{1}{2}\varepsilon_{\mu\nu} F^{\mu\nu}. \tag{4.24}$$

This effective action was first presented for $\mathcal{N} = (2,2)$ and $\mathcal{N} = (0,2)$ supersymmetric $CP(N-1)$ models in [28]. Here we generalize it for the $\tilde{\mu}$-deformed $CP(N-1)$ model (2.13). The potential $V(\sigma)$ here can be obtained from (3.9) by eliminating D by virtue of its equation of motion.

Coefficients in front of A_μ and σ kinetic terms are finite after renormalization reflecting Witten's observation that these fields become physical [18]. The last term in (4.23) is $A_\mu - \sigma$ induced by the chiral anomaly. Because of this mixing, the would-be massless photon and the phase of σ acquire a mass (4.6) already in unperturbed theory at $\tilde{\mu} = 0$. This term is also present when we switch on the deformation.

[3]In this subsection we will use the Minkowski formulation with $g^{\mu\nu} = \text{diag}\{+,-\}$, and for the Levi-Civita symbol $\varepsilon_{01} = -\varepsilon^{01} = +1$.

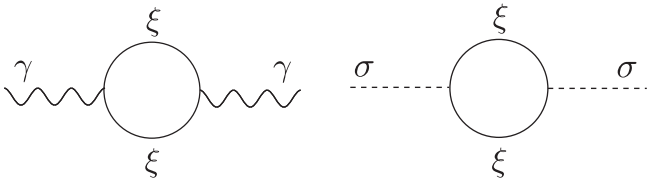

(a) Photon wave function renormalization

(b) Scalar wave function renormalization

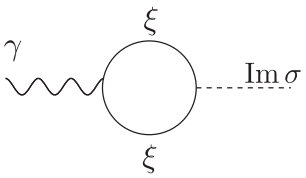

(c) Photon-scalar mixing

FIG. 4. Contributions to the effective action.

Coefficients in this effective action come from loops. We take the low-energy limit when the external momenta are small. There are several contributions. Photon wave function renormalization comes from the diagram on Fig. 4(a) and a similar graph with a bosonic loop. Wave function renormalizations for $\Re\sigma$ and $\Im\sigma$ come from the diagram on Fig. 4(b) and also a similar graph with a bosonic loop. Finally, the mixing term is given by the diagram on Fig. 4(c). For the mass distribution (2.3) and the vacuum with $\Im\langle\sigma\rangle = 0$, the normalization factors are

$$\frac{1}{e^2_{\Re\sigma}} = \frac{1}{4\pi}\sum_{k=0}^{N-1}\left[\frac{1}{3}\frac{M^2_{\xi_k}+2(\Im m_k)^2}{M^4_{\xi_k}}+\frac{2}{3}\frac{(\sqrt{2}\langle\sigma\rangle-\Re m_k)^2}{m^4_{n_k}}\right],$$
$$\frac{1}{e^2_{\Im\sigma}} = \frac{1}{4\pi}\sum_{k=0}^{N-1}\left[\frac{1}{3}\frac{3M^2_{\xi_k}-2(\Im m_k)^2}{M^4_{\xi_k}}+\frac{2}{3}\frac{(\Im m_k)^2}{m^4_{n_k}}\right],$$
$$\frac{1}{e^2_{\gamma}} = \frac{1}{4\pi}\sum_{k=0}^{N-1}\left[\frac{1}{3}\frac{1}{m^2_{n_k}}+\frac{2}{3}\frac{1}{M^2_{\xi_k}}\right],$$
$$b_{\gamma,\Im\sigma} = \frac{1}{2\pi}\sum_{k=0}^{N-1}\frac{\sqrt{2}\langle\sigma\rangle-m_k-\lambda(\tilde{\mu})}{M^2_{\xi_k}}. \tag{4.25}$$

Here, $M^2_{\xi_k}$ and $m^2_{n_k}$ are the masses of the ξ_k and n_k fields, respectively:

$$M^2_{\xi_k} = |\sqrt{2}\langle\sigma\rangle - m_k - \lambda(\tilde{\mu})|^2,$$
$$m^2_{n_k} = i\langle D\rangle + \upsilon(\tilde{\mu})\Delta m_k + |\sqrt{2}\langle\sigma\rangle - m_k|^2. \tag{4.26}$$

We present details of this calculation in Appendix A.

Next we diagonalize the photon-σ mass matrix in (4.23); see Appendix B. As we already mentioned, this diagonalization shows that the photon acquires a massless component as soon as we switch on $\tilde{\mu}$. This component is responsible for the presence of the constant electric field in quasivacua. This constant electric field gives rise to a second mechanism of quasivacua splitting; see (B10). This effect is small at small $\tilde{\mu}$ but becomes dominant at larger $\tilde{\mu}$ above the phase transition point. This result can also be derived in a different way which we consider in the next subsection.

2. Coulomb potential and vacuum energies

In this section we study the formation of a constant electric field in a quasivacuum generalizing a method developed by Witten in [18] for the $\mathcal{N} = (2,2)$ supersymmetric $CP(N-1)$ model.

Let us start with the effective action (4.23) taking into account the presence of the trial matter charges,

$$S_{\text{eff}} = \int d^2x\left\{-\frac{1}{4e^2_\gamma}F^2_{\mu\nu} - \sqrt{2}b_{\gamma,\Im\sigma}\Im\sigma F^* + j_\mu A^\mu\right\}. \tag{4.27}$$

Consider a stationary pointlike kink at $x = x_0$ with electric charge $+1$ described by the current $j_\mu = (\delta(x-x_0), 0)$ and $F^* = -\frac{1}{2}\varepsilon^{\mu\nu}F_{\mu\nu} = \partial_0 A_1 - \partial_1 A_0$.

We have the equation of motion for the photon,

$$-\frac{1}{e^2_\gamma}\partial_x\mathcal{E} - \sqrt{2}b_{\gamma,\Im\sigma}\partial_x\Im\sigma = -j_0, \tag{4.28}$$

where

$$\mathcal{E} = F_{01} \tag{4.29}$$

is the electric field strength. Integrating over the spatial coordinate we obtain

$$\frac{1}{e^2_\gamma}(\mathcal{E}(\infty)-\mathcal{E}(-\infty)) + \sqrt{2}b_{\gamma,\Im\sigma}(\Im\sigma(\infty)-\Im\sigma(-\infty)) = 1. \tag{4.30}$$

In the supersymmetric case $\tilde{\mu} = 0$ the photon is massive, so there is no constant electric field, $\mathcal{E}(\infty) = \mathcal{E}(-\infty) = 0$. Therefore we have

$$\sqrt{2}b_{\gamma,\Im\sigma}(\Im\sigma(\infty)-\Im\sigma(-\infty)) = 1. \tag{4.31}$$

Since

$$b_{\gamma,\Im\sigma} = \frac{1}{2\pi}\frac{N}{\Lambda} \tag{4.32}$$

[see Eq. (4.25)] for $\tilde{\mu} = 0$ we get

$$\sqrt{2}(\Im\sigma(\infty)-\Im\sigma(-\infty)) = 2\pi\frac{\Lambda}{N}, \tag{4.33}$$

which, if we set $\tau(-\infty) = -\Lambda$ for the true vacuum, is an approximation of

$$\tau(\infty) = -\Lambda e^{\frac{2\pi i}{N}} \tag{4.34}$$

for the value of σ VEV in the first quasivacuum; see (4.10). This result for the $\mathcal{N} = (2,2)$ case has been derived long ago by Witten [18] showing the presence of N vacua and kinks interpolating between them.

Now, consider small deformations in the Eq. (4.30) for a kink interpolating between the ground state (4.17) at $x = -\infty$ and the first quasivacuum (4.18) at $x = +\infty$. Setting $\mathcal{E}(-\infty) = 0$ we get from (4.30)

$$\frac{1}{e_\gamma^2}\mathcal{E}(\infty) + \sqrt{2} b_{\gamma,\Im\sigma}(\Im\sigma(\infty) - \pi) = 1. \tag{4.35}$$

Using (4.18) and (4.32) we obtain for the electric field strength

$$\mathcal{E}(\infty) = e_\gamma^2 \frac{\lambda}{\Lambda} \ln \frac{m_G}{\Lambda}. \tag{4.36}$$

We see that the kink produces a constant electric field now. This gives the contribution to the energy density splitting between the first quasivacuum and the true vacuum

$$(E_1 - E_0)|_{\mathcal{E}} = \frac{1}{2e_\gamma^2}\mathcal{E}^2 = \frac{2\pi}{N}\left(\lambda \ln \frac{m_G}{\Lambda}\right)^2. \tag{4.37}$$

This coincides with the result (B10) obtained from the photon-σ diagonalization. This contribution is small compared to the σ splitting given by (4.11) at small $\tilde{\mu}$.

C. Second order phase transition

As we learned so far, the vacuum energy (or, rather, energy splitting between the ground state and the first quasivacuum) has two contributions, which depend on the parameter

$$\omega = \frac{\lambda(\tilde{\mu})}{\Lambda} \ln \frac{m_G}{\Lambda}. \tag{4.38}$$

The first contribution is the splitting of different quasiminima σ_i of the effective potential (4.11). When we turn on ω (i.e., supersymmetry breaking parameter $\tilde{\mu}$), this contribution at first grows linearly with ω, and then drops to zero when the σ quasiminima disappear.

The second contribution comes from the electric field of charged kinks interpolating between the quasivacua; see (B10) and (4.37). This contribution at first grows as ω^2, and at the point when the first σ quasivacuum disappears, the electric field jumps up to saturate (4.30).[4]

[4]This jumping is not seen from the propagator considerations (B10) since it holds only perturbatively near the true vacuum and does not take into account the presence of σ quasivacua.

The jumping point is the same for these two contributions, and it is where a phase transition occurs. The corresponding critical value is $\omega_c \sim 1$; i.e., [cf. (4.22) and (4.19)]

$$\lambda_{\text{crit}} = \lambda(\tilde{\mu}_{\text{crit}}) \sim \frac{\Lambda}{\ln \frac{m_G^2}{\Lambda^2}}. \tag{4.39}$$

Full vacuum energy is the sum of these two contributions, and on general grounds we expect that it does not jump. Rather, its first derivative is discontinuous, and the phase transition must be of the second order. Numerical calculations confirm this; see Fig. 5. At the point where the quasivacuum disappears, the two contributions to the vacuum energy jump, and the magnitudes are just right for the total sum to stay continuous. However, we must point out that we do not have enough accuracy for the detailed study of the vicinity of the transition point. The point is that we can trust our formula for the arg τ potential (4.5) only in the vicinities of the minima (4.4), and we do not know the exact form of this potential in regions between any of two adjacent minima.

At small deformations, the main contribution to the vacuum energy is σ-quasivacua splitting (4.11). After the transition point, vacuum energy is determined solely by the kink electric field. As we reviewed in Sec. II A, it is the electric field that is responsible for the quasivacuum energy splittings in the nonsupersymmetric $CP(N-1)$ model. This is consistent with our results, since at large $\tilde{\mu}$ above the phase transition point our model flows to the nonsupersymmetric $CP(N-1)$ model.

To conclude this section we note that parameter ω relevant for the quasivacua splitting is enhanced by the large logarithm $\ln m_G/\Lambda \gg 1$. Hence the phase transition point occurs at $\tilde{\mu}_c \sim \lambda_c$ given by (4.39), much smaller than $\tilde{\mu} \sim \Lambda$. These are even smaller values of $\tilde{\mu}$ as compared to m_G since we assume $m_G \gg \Lambda$ in order to keep the bulk theory at weak coupling. At these small values of $\tilde{\mu}$ we are way below the scale of adjoint matter decoupling in the bulk theory which occurs at $\tilde{\mu} \gg m_G$. In particular, the scale Λ of the world sheet theory is close to Λ_{4d} rather than to its large-$\tilde{\mu}$ asymptotic values (2.27).

D. Large deformations

As we increase the deformation parameter $\tilde{\mu}$, the fermion mass λ approaches the UV cutoff scale m_G, and we can expect that the fermions become very heavy and decouple, effectively taking no part in the dynamics. Therefore, our theory should become the nonsupersymmetric $CP(N-1)$ model (2.1). The VEV of the τ field should become zero.

We can check this directly using our effective potential (4.3). Indeed, assume that $\tau \ll \lambda \sim m_G$. Then we can expand (4.3) to obtain

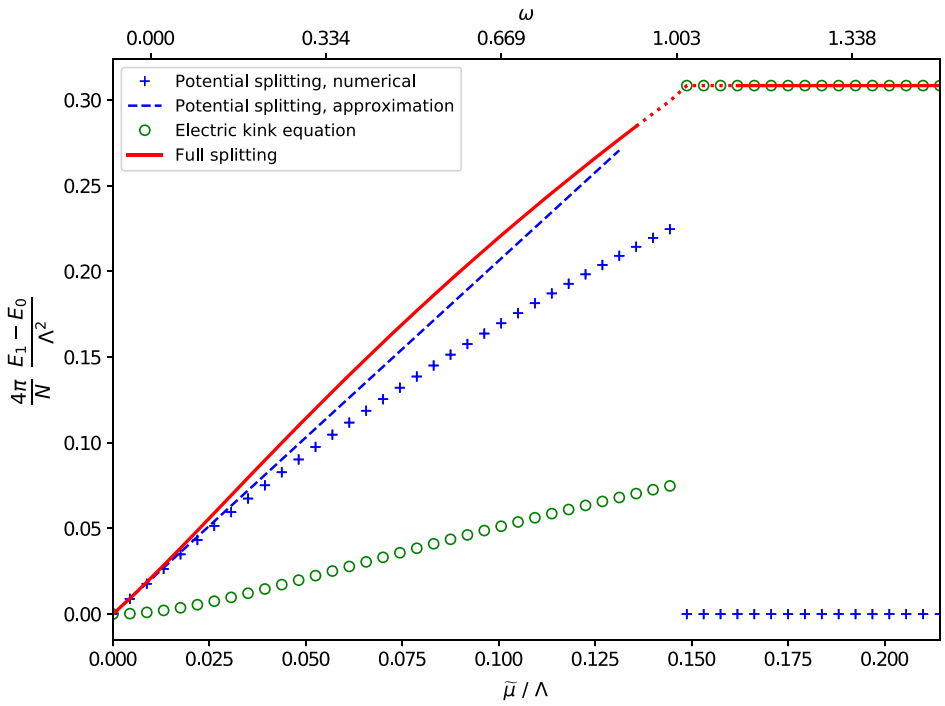

FIG. 5. Different contributions to the vacuum energy. The vertical axis is labeled by the rescaled energy splitting $E_1 - E_0$. Values of the deformation parameter $\tilde{\mu}$ are on the lower horizontal axis (in the units of Λ), while the upper horizontal axis represents the parameter ω (4.38). Green circles denote the contribution from the electric field [solution of (4.30), given by (4.37) below the phase transition point], + signs represent the splitting from the potential (4.3) [the blue dashed line is the approximation (4.11)]. The solid red line is the sum of these two contributions. Phase transition occurs at $\omega \approx 1$ where the full energy displays a discontinuity of the first derivative. Our model does not allow us to obtain exact results in the vicinity of the phase transition point, and we have to extrapolate from the left and from the right (red dotted line continuing the solid red curve).

$$\mathcal{V}_{\text{eff}} = \frac{N}{4\pi} iD\left[1 - \ln\frac{iD + |\tau|^2}{\Lambda^2}\right] + \frac{N}{4\pi}|\tau|^2\left[1 - \ln\frac{iD + |\tau|^2}{m_G^2}\right] - \frac{N}{4\pi}\cdot 2\Re\tau\cdot\lambda\ln\frac{\lambda^2}{m_G^2} - \frac{N}{4\pi}\lambda^2\left(1 - \ln\frac{\lambda^2}{m_G^2}\right). \quad (4.40)$$

Minimizing this potential we obtain

$$\tau \approx -\lambda\frac{\ln(m_G/\lambda)}{\ln(m_G/\Lambda)}. \quad (4.41)$$

This formula turns out to be pretty good compared to the exact numerical solution; see Fig. 6(a). As λ approaches the UV cutoff scale m_G, the VEV of τ vanishes. The first term in (4.40) reduces to the effective potential for the nonsupersymmetric $CP(N-1)$ model, while the last term gives a vacuum energy shift. At $\lambda = m_G$, the vacuum energy is

$$E_{\text{vac,UV}} = \frac{N}{4\pi}(\Lambda^2 - m_G^2). \quad (4.42)$$

This is in agreement with the Appelquist-Carazzone decoupling theorem [30], which states that the effect of heavy fields is limited to the renormalization of physical quantities. Note that since the supersymmetry is explicitly broken in the world sheet theory by fermion masses, the vacuum energy is not positively defined.

The vacuum energy above is a quantum correction to the classical expression for the non-Abelian string tension in the bulk theory. The latter was derived in [16], and together with (4.42) it can be written as

$$T = \frac{2\pi}{\ln\frac{m_G^2}{m^2}}\frac{m_G^2}{g^2} + \frac{N}{4\pi}(\Lambda^2 - m_G^2). \quad (4.43)$$

We see that the second term here is just an $O(g^2)$ correction to the classical formula.

At intermediate values of λ we were able to study this model only numerically. The results are presented on Fig. 6. They show the dependence of $\langle\sigma\rangle$ and E_{vac} on the heavy fermion mass λ. One can see that indeed the VEV of τ vanishes at very large λ. Note that we will have $\langle iD\rangle < 0$ in a wide range of λ, but this does not lead to an instability because, according to (4.12), the mass of the n field is always positive.

E. Split mass case

The results obtained in the previous section can be generalized to the case $\Delta m_{i0} \neq 0$. Consider the masses on a

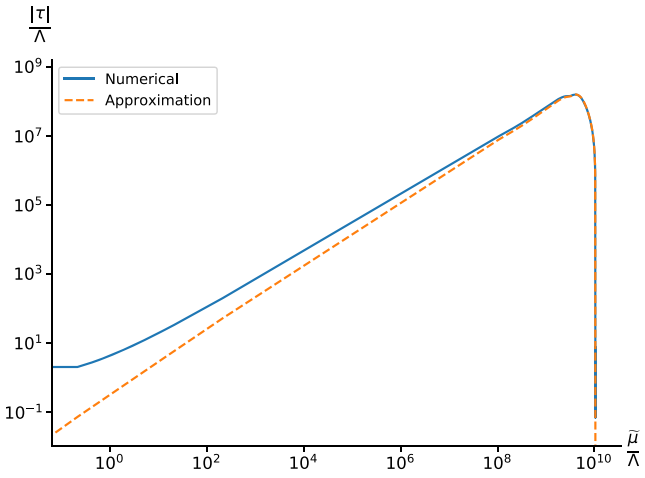

(a) VEV of τ as a function of $\tilde{\mu}$, double log scale.

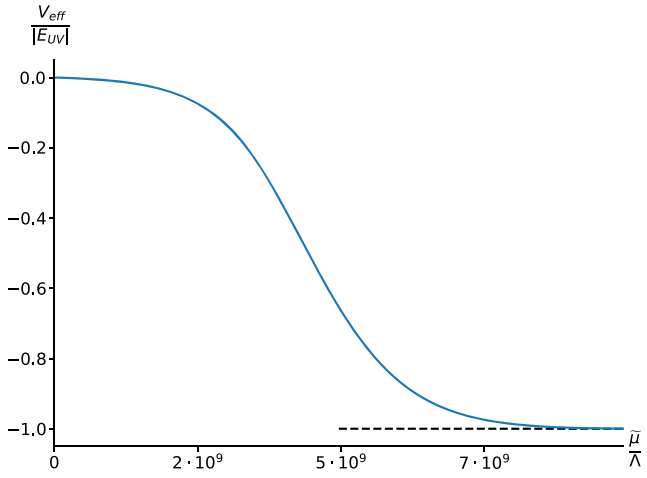

(b) Vacuum energy as a function of $\tilde{\mu}$, log scale

FIG. 6. Numerical results for the VEV of τ and vacuum energy at large deformations $\lambda \gg 1$. (a) We have VEV of τ. The dashed line shows the approximate solution (4.41), while the solid line is the result of numerics. One can see that τ indeed vanishes at $\lambda(\tilde{\mu}) = m_G$. (b) We have E_{vac}. The dashed line shows its asymptotic value E_{UV} given by (4.42). In the numerical procedure we had set $m_G/\Lambda = 10^{10}$.

circle (2.3), with the radius Δm as the mass scale of our model.

If we fix some Δm and start increasing $\tilde{\mu}$ [and, therefore, $\lambda(\tilde{\mu})$], our model exhibits similar behavior as in the case $\Delta m = 0$. At $\tilde{\mu} = 0$ the supersymmetry is unbroken, and there are N degenerate vacua. When we switch on the deformation, the degeneracy is lifted, and eventually all lifted quasivacua decay, which signifies a phase transition. The set of the phase transition points represents a curve on the $(\mu, \Delta m)$ plane; see Fig. 7.

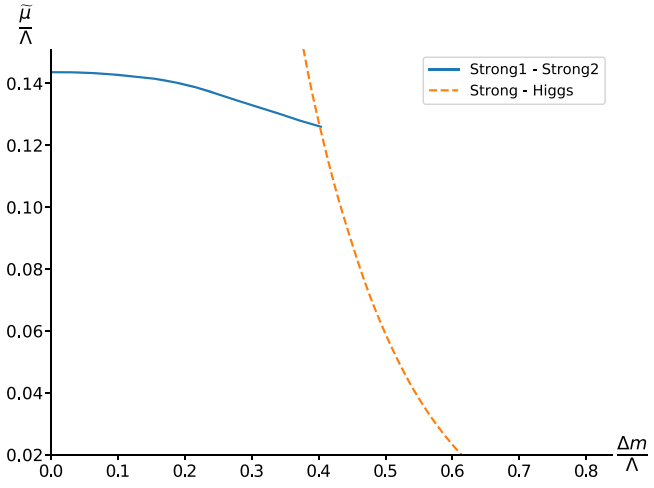

FIG. 7. Phase transition line between two strong coupling regimes (shown in solid blue). The dashed line is the phase transition line between the Strong coupling and Higgs regimes; see Sec. V B. This plot is a result of numerical calculations for $N = 16$.

Qualitatively, we see nothing new. However, when Δm is large enough, the theory goes through the phase transition from the strong coupling phase into a weak coupling phase, the so-called "Higgs" phase. This will be the subject of the next section.

V. HIGGS REGIME

When the mass difference Δm exceeds some critical value, the theory appears in the Higgs phase. This phase is characterized by a nonzero VEV of n. At very weak coupling, we can use the classical Lagrangian (2.13) to find the vacuum solution,

$$n_0^2 = 2\beta, \qquad \sqrt{2}\sigma = m_0, \qquad iD = 0. \tag{5.1}$$

The vacuum energy is classically zero.

In the supersymmetric case $\tilde{\mu} = 0$ the solution for σ is exact at large N. Moreover, at very large Δm the coupling constant $1/\beta$ is small (frozen at the scale Δm) and quantum corrections to the classical vacuum solution (5.1) are small.

However, at nonzero $\tilde{\mu}$ and for $\Delta m \gtrsim \Lambda$, things become more complicated, as we can no longer rely on the classical equations. Generally speaking, solution (5.1) receives $\Lambda/\Delta m$ and $\tilde{\mu}/\Lambda$ corrections. We have to work with the quantum equations (3.12)–(3.14), and most of the results presented in this section were obtained from numerical calculations.

First of all, we wish to check that the one-loop potential that we derived (3.9) is compatible with the classical limit. Consider the limit of large $\Delta m \gg \Lambda$ with some $\tilde{\mu}$ fixed. We can expand the vacuum Eqs. (3.12)–(3.14) in powers of $\Lambda/\Delta m$ and easily derive an approximate solution for the ground state VEV,

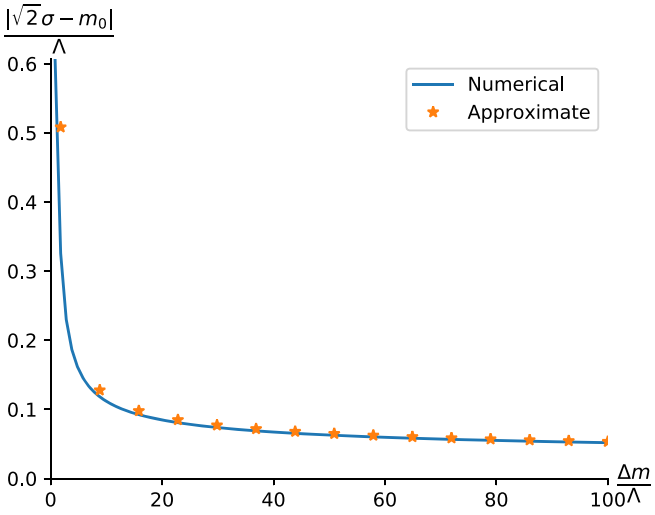

FIG. 8. The VEV of $\tau = \sqrt{2}\sigma - m_0$ as a function of Δm. The solid line is the exact result of numerical calculation, while stars represent the approximate formula (5.2). Here $\tilde{\mu} = \Lambda$. In numerical calculations we used $N = 16$. One can see that indeed, as Δm grows, the VEV of $\sqrt{2}\sigma$ goes to its classical value m_0.

$$\sqrt{2}\sigma - m_0 \approx -\lambda(\tilde{\mu})\frac{\ln\frac{m_G}{\Delta m}}{\ln\frac{\Delta m}{\Lambda}}. \tag{5.2}$$

Figure 8 presents our results for the VEV of σ. One can see that the formula (5.2) gives a very good approximation [see also Fig. 10(a)]. At large Δm we indeed have $\sqrt{2}\sigma \approx m_0$.

A. Quasivacua

Solution (5.1) is just one of the possible vacuum states in the Higgs phase. In the supersymmetric case $\tilde{\mu} = 0$ there are N degenerate vacua as dictated by the Witten index. In [26] it was shown that the theory at large Δm is in the Higgs phase where different components of the N-plet n_i develop a VEV. These vacua are characterized by

$$\langle\sqrt{2}\sigma\rangle = m_{i_0}, \quad \langle|n_{i_0}|^2\rangle = 2\beta, \quad i_0 = 0,\ldots,N-1. \tag{5.3}$$

Moreover, there are kinks interpolating between these vacua.

As we switch on the deformation parameter $\tilde{\mu}$, these vacua split, and at small $\tilde{\mu}$ we have one true ground state (5.1) and $N-1$ quasivacua. Let us first consider this picture from the classical Lagrangian (2.13). The classical potential is

$$\mathcal{V}_{\rm cl}(n,\sigma,D) = iD(\bar{n}_i n^i - 2\beta) + \sum_i |\sqrt{2}\sigma - m_i|^2|n^i|^2 + v(\mu)\sum_i \Re\Delta m_{i0}|n^i|^2. \tag{5.4}$$

Let us derive the mass spectrum in the vicinity of a vacuum $\sqrt{2}\sigma = m_{i_0}$ for some i_0. Then $n^i, i \neq i_0$ are small, while

$$n_{i_0} = \sqrt{2\beta} + \delta n_{i_0}. \tag{5.5}$$

From the D-term condition

$$\delta n_{i_0} \approx -\frac{1}{2\cdot 2\beta}\sum_{i\neq i_0}|n^i|^2, \tag{5.6}$$

and the potential (5.4) becomes

$$\begin{aligned}\mathcal{V}_{\rm cl} &\approx \sum_{i\neq i_0}|m_i - m_{i_0}|^2|n^i|^2 + v(\mu) \\ &\quad\times\sum_{i\neq i_0}\Re(m_i - m_0)|n^i|^2 - v(\mu)\Re(m_{i_0} - m_0)\sum_{i\neq i_0}|n^i|^2 \\ &= \sum_{i\neq i_0}|n^i|^2[|m_i - m_{i_0}|^2 + v(\mu)\Re(m_i - m_{i_0})]\end{aligned} \tag{5.7}$$

so that the mass of the n^i particle is

$$M_i^2 = |m_i - m_{i_0}|^2 + v(\mu)\Re(m_i - m_{i_0}). \tag{5.8}$$

If M_i^2 were to turn negative for some i, this would signify that the vacuum under consideration is unstable. This happens for all $i_0 \neq 0$ if the deformation is large enough because there are always some i with $\Re(m_i - m_{i_0}) < 0$.

To be more concrete, consider our choice of the masses (2.3). Then for the vacuum $i_0 = 0$ we have $\Re(m_i - m_0) > 0$ for all $i \neq 0$, and this vacuum is stable. However, the vacua $0 < i_0 < N/2$ can be shown to become unstable when the deformation parameter hits the critical value

$$v(\mu_{{\rm crit},i_0}) = 2\Delta m\frac{1-\cos(\frac{2\pi}{N})}{\cos(\frac{2\pi(i_0-1)}{N}) - \cos(\frac{2\pi i_0}{N})} \approx \frac{4\pi}{N}\frac{\Delta m}{\sin(\frac{2\pi i_0}{N})}. \tag{5.9}$$

The last step is the large N approximation. A similar statement holds for the quasivacua $N/2 < i_0 < N$, while the quasivacuum number $i_0 = N/2$ (for even N) decays when $v(\mu_{{\rm crit},N/2}) = 2\Delta m$. When $\tilde{\mu}$ is above this critical value, the theory has a unique vacuum, and there are no kinks left.

These quasivacua are seen from the one-loop potential as well. Following [26], we can study these quasivacua as follows. Recall that deriving the effective potential (3.9) we assumed that $n \equiv n_0$ can develop a VEV. Now to study quasivacua we assume that n_{i_0} is nonzero and integrate out the other components of n^i. Numerical calculations show that the resulting effective potential has a minimum for small deformations, but this minimum fades away at large $\tilde{\mu}$; see Fig. 9. On the plot of Fig. 9(a), this corresponds to the fact that $|n|^2$ rapidly drops near the phase transition point. Figure 9(b) shows that the quasivacua are degenerate when supersymmetry is unbroken, and that the quasivacuum energy is indeed higher than that of the true ground state.

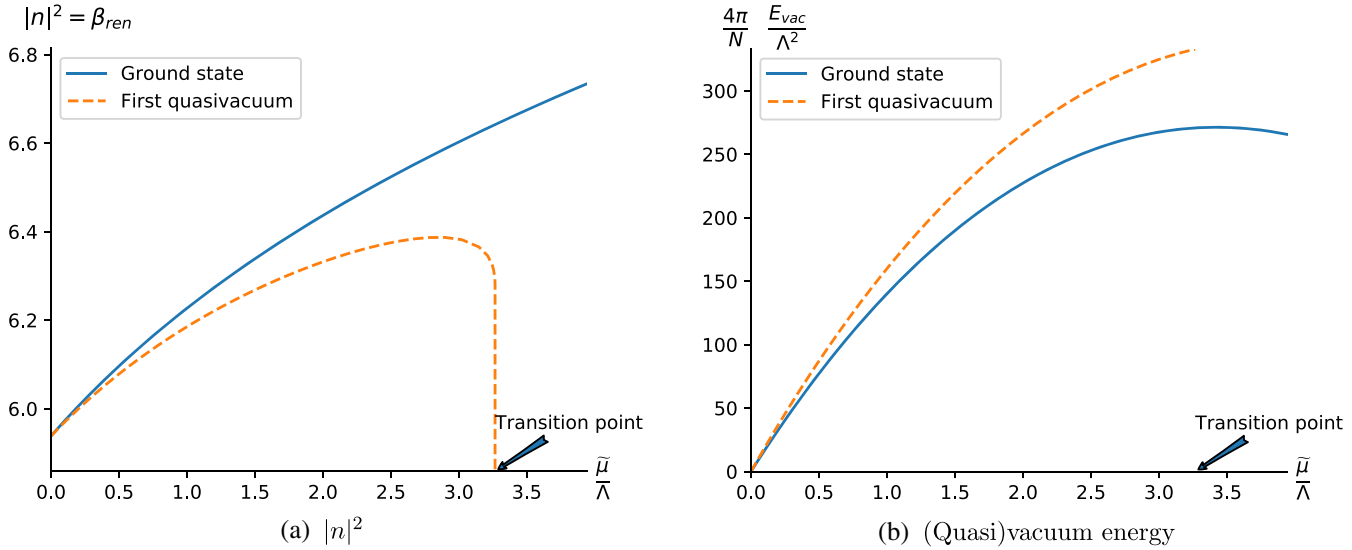

(a) $|n|^2$ (b) (Quasi)vacuum energy

FIG. 9. Example of kinks-nokinks phase transition for $\Delta m/\Lambda = 10$. The blue solid line refers to the true ground state $i_0 = 0$, the orange dashed line represents the first quasivacuum $i_0 = 1$. The value of the deformation parameter $\tilde{\mu}$ is on the horizontal axis (in the units of Λ), the phase transition point is indicated by an arrow. Both figures are the result of numerical calculations at $\Delta m/\Lambda = 10$, $N = 16$.

Figure 11 shows the phase transition curve. One can see that the classical formula (5.9) is valid only if we set $\lambda = 0$ in (2.13), but it is completely inadequate when the fermions gain extra mass. As we see from Fig. 11(b) massive fermions magnify the effect.

Let us derive a better theoretical formula for the phase transition curve. Consider, for example, the first quasivacuum $i_0 = 1$. Then in the expression for β_{ren} (3.12) we will have $\Delta m_{i1} = m_i - m_1$ instead of Δm_{i0}. Then $\Re\Delta m_{01} < 0$, and for the phase transition point we can take roughly the point when $\beta_{\text{ren}} \to -\infty$, i.e.,

$$iD + v(\tilde{\mu})\Re\Delta m_{01} + |\sqrt{2}\sigma - m_0|^2 = 0. \qquad (5.10)$$

Using (2.23), (2.24), (5.2), and an analog of (3.13), one can show that the phase transition occurs at the point

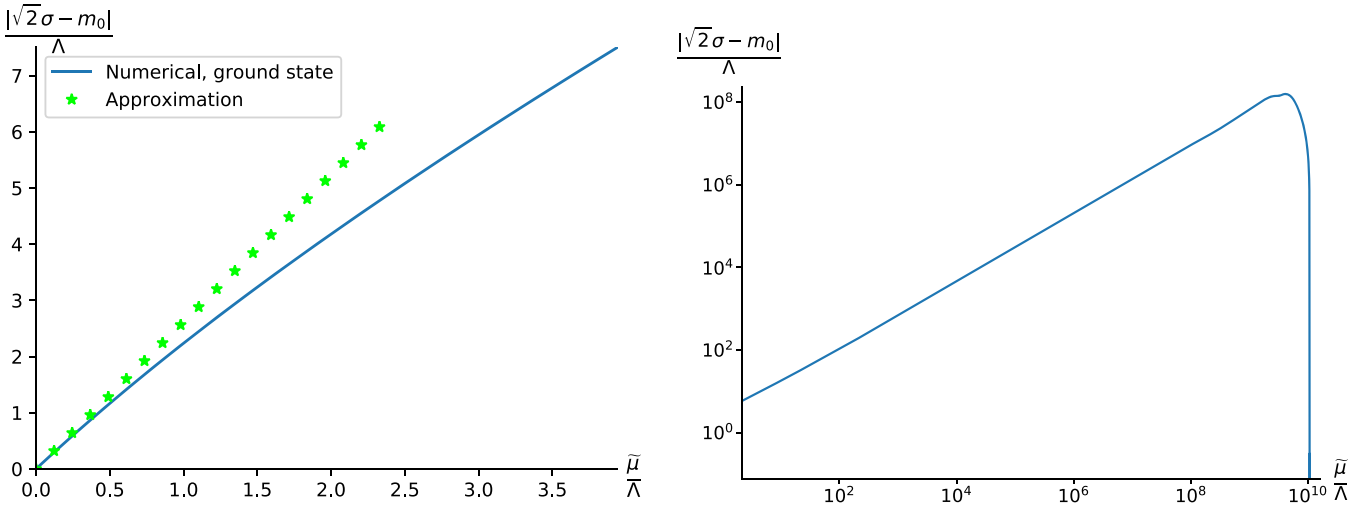

(a) $|\sqrt{2}\sigma - m_0|$ at small $\tilde{\mu}$. (b) $|\sqrt{2}\sigma - m_0|$ at large $\tilde{\mu}$.

FIG. 10. The VEV of $\sqrt{2}\sigma - m_0$ at different scales. (a) Small $\tilde{\mu}$. The solid blue line is the result of numerical calculations, and the green stars show the approximate formula (5.2). (b) Large-$\tilde{\mu}$ behavior (in double log scale). One can see that as $\tilde{\mu} \to m_G$ we indeed have $\sqrt{2}\langle\sigma\rangle \to m_0$. The plots were made for fixed $\Delta m/\Lambda = 10$, $m_G/\Lambda = 10^{10}$, $N = 16$

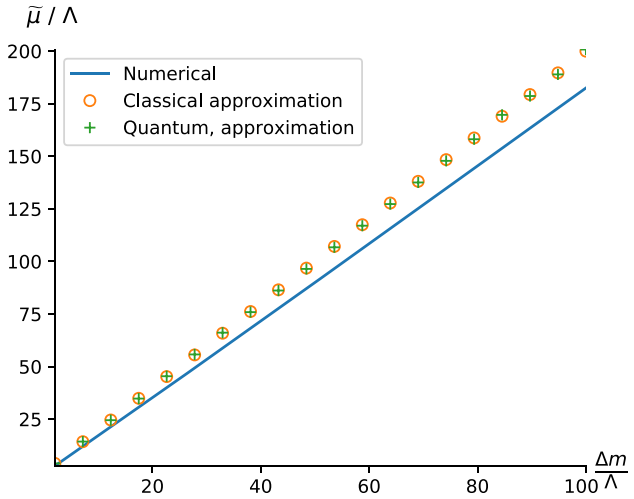

(a) Agreement with the classical formula (4.9) if we set $\lambda = 0$

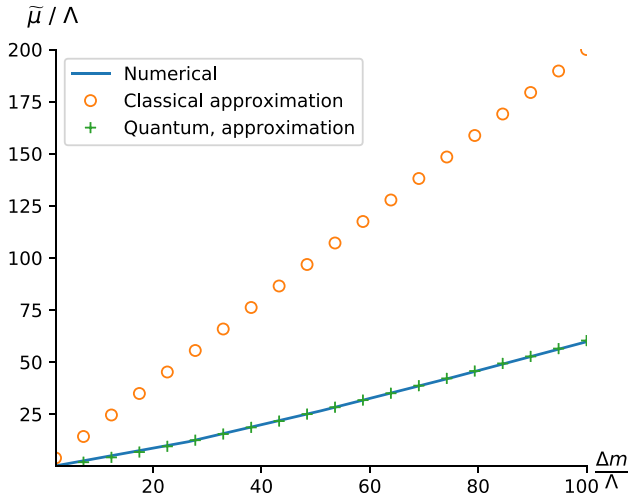

(b) Presence of λ magnifies the effect

FIG. 11. Kinks-nokinks phase transition line. Δm on the horizontal axis, and $\tilde{\mu}$ on the vertical axis. The solid blue line is the result of the numerical calculation of the curve where all quasivacua have decayed leaving the single true ground state. Orange circles represent the classical formula (5.9), green + are the quantum approximation (5.11). (a) If we set $\tilde{\lambda}_0 = 0$, we indeed get good agreement with the classical formula (5.9). However, the real scenario (b) is better described by formula (5.11).

$$\tilde{\mu}_{\rm crit} \approx \frac{2\Delta m}{1+\tilde{\lambda}_0 \frac{\ln m_G/\Delta m}{\ln \Delta m/\Lambda}}. \tag{5.11}$$

At very large values of $\tilde{\mu}$ all but one vacua have decayed, and the world sheet theory flows to the non-supersymmetric model. In this limit the VEV of $\sqrt{2}\sigma$ again tends to m_0. Indeed, at large $\tilde{\mu}$ we can solve the vacuum equations (3.12)–(3.14) approximately, and using the expression for Λ (2.27), we find that

$$\sqrt{2}\sigma - m_0 \sim \frac{\Delta m m_G^2}{\tilde{\mu}^2} \ln\frac{\tilde{\mu}}{\Delta m} \ln\frac{\tilde{\mu}}{m_G}, \tag{5.12}$$

which vanishes at large values of $\tilde{\mu}$. This is supported by numerical calculations; see Fig. 10(b).

B. Strong-Higgs phase transition

It was found in [21,26] that for the nonsupersymmetric $CP(N-1)$ model (2.1) and for the supersymmetric $CP(N-1)$ model (2.7) a phase transition between strong coupling and Higgs phases occurs at the point $\Delta m = \Lambda$. At large Δm the theory is weakly coupled and in the Higgs phase, while at small Δm we have a strong coupling phase. We expect similar behavior in our deformed model (2.13).

Following [21,26] we identify the Higgs–strong coupling phase transition with a curve where $|n_0^2| = 2\beta_{\rm ren}$ turn negative. Thus we are looking for the solutions of the equation

$$\beta_{\rm ren} = 0, \tag{5.13}$$

where $\beta_{\rm ren}$ is given by (3.12), see Fig. 12(a). See also Fig. 13 for the behavior of the ground state energy.

In $\mathcal{N} = (2,2)$ the supersymmetric model at $\tilde{\mu} = 0$ a phase transition is at $\Delta m = \Lambda$ [26]. The case $\tilde{\mu} \neq 0$ is more complicated. We were not able to solve the vacuum equations (3.12)–(3.14) exactly, but an approximate calculation can be done in regions of small and very large $\tilde{\mu}$.

First consider the region $\tilde{\mu} \lesssim \Lambda$ and assume that the VEV of σ is real valued (this assumption is correct for the true ground state anyway). Then, using (3.13) and the identity

$$\prod_{k=1}^{N-1} \sin\left(\frac{\pi k}{N}\right) = \frac{N}{2^{N-1}}, \tag{5.14}$$

we can rewrite (3.12) as

$$2\beta_{\rm ren} = \frac{2(N-1)}{4\pi}\left(\ln\frac{\Delta m}{\Lambda} + \frac{1}{N-1}\ln N + \frac{1}{2}\ln\left(1 + \frac{v(\tilde{\mu}) - 2(\sqrt{2}\sigma - m_0)}{2\Delta m}\right)\right). \tag{5.15}$$

Equating this to zero yields

$$v(\tilde{\mu}) - 2(\sqrt{2}\sigma - m_0) = 2\Delta m\left(\left(\frac{\Lambda}{\Delta m}\right)^2 N^{-\frac{2}{N-1}} - 1\right). \tag{5.16}$$

At small deformations we can use the approximation $v(\tilde{\mu}) \approx \tilde{\mu}$; see (2.23). Moreover, in the strong coupling phase at fixed $\tilde{\mu}$, the VEV of σ does not depend on Δm [this is exactly true in the supersymmetric and pure

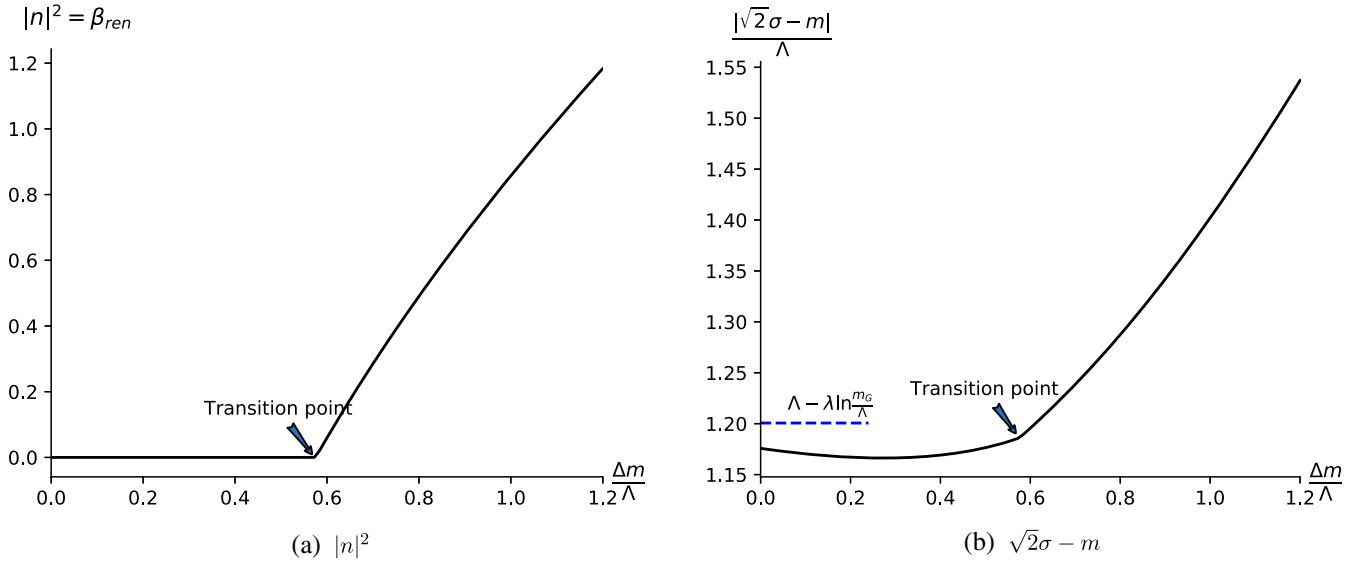

(a) $|n|^2$ (b) $\sqrt{2}\sigma - m$

FIG. 12. Strong—Higgs phase transition: VEVs. The curves show an example of the phase transition for fixed $\tilde{\mu}/\Lambda = 0.03$, $N = 16$. Mass scale Δm is on the horizontal axis. Location of the phase transition point is indicated with an arrow. (b) The position approximate strong coupling VEV (4.17) is signified on the vertical axis by a blue dashed line. One can see that the character of the phase transition is qualitatively the same as in the pure nonsupersymmetric (2.1) and supersymmetric (2.7) models; see [21,26].

nonsupersymmetric $CP(N-1)$ models], and we can use $\Delta m = 0$ approximation (4.17) right up until the phase transition point, see Fig. 12(b). Then, from (5.16) we can actually derive the equation for the phase transition curve:

$$\tilde{\mu}_{\text{crit}} = \frac{2\frac{\Lambda^2}{\Delta m} N^{-\frac{2}{N-1}} - \Lambda - \Delta m}{1 + 2\tilde{\lambda}_0 \ln \frac{m_G}{\Lambda}}, \tag{5.17}$$

or, sending $N \to \infty$,

$$\tilde{\mu}_{\text{crit}} = \frac{(2\Lambda + \Delta m)(\Lambda - \Delta m)}{\Delta m(1 + 2\tilde{\lambda}_0 \ln \frac{m_G}{\Lambda})}. \tag{5.18}$$

These formulas give a good approximation for the phase transition curve; see Fig. 14. We see that with $\tilde{\mu}_{\text{crit}}$ growing,

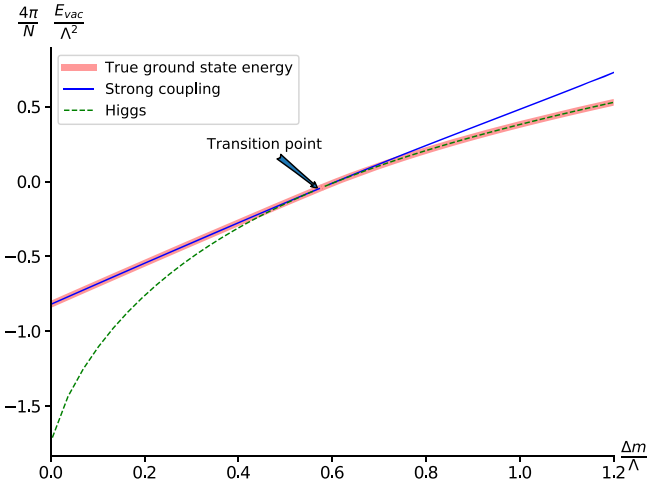

FIG. 13. Strong-Higgs phase transition: energy. The red thick line is a numerical result for the ground state vacuum energy. The solid blue line to the right of the phase transition point is a numerical continuation of the strong coupling vacuum energy into the Higgs regime. Vice versa, the dashed green line below the phase transition is a numerical continuation of the Higgs regime vacuum energy into the strong coupling (corresponds to the unphysical "state" with formally $|n|^2 < 0$). At the phase transition point these two curves touch, and $|n|^2 = 0$. This plot is qualitatively the same as in the pure nonsupersymmetric (2.1) and supersymmetric (2.7) models; see [21,26]. In the numerical procedure we have set $\tilde{\mu}/\Lambda = 0.03$, $N = 16$.

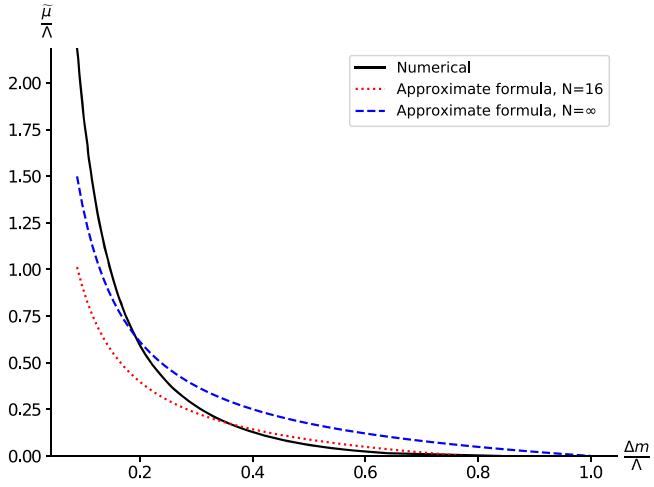

FIG. 14. Strong-Higgs phase transition line. Δm on the horizontal axis, $\tilde{\mu}$ on the vertical axis. The solid black line is the numerical result for $N = 16$. The dotted red line is the $N = 16$ approximate formula (5.17). The dashed blue line is the $N \to \infty$ approximate formula (5.18).

$\Delta m_{\rm crit}$ monotonically decreases. Moreover, comparing (5.17) and (5.18), we can test the validity of our numerical calculations compared to the large-N limit, as the numerics is done, of course, for a finite N.[5]

In the region of large deformations, $\tilde{\mu} \gg m_G$. We have

$$2\beta_{\rm ren} \sim \frac{N}{4\pi} \ln \frac{v(\mu_{\rm crit})\Delta m_{\rm crit} + \Delta m_{\rm crit}^2}{\Lambda_{2d}^2} = 0, \tag{5.19}$$

where Λ_{2d} is exponentially small given by (2.22). From (2.23) and (2.27) we derive up to logarithmic factors

$$\Delta m_{\rm crit} \sim \frac{(\Lambda_{4d}^{\mathcal{N}=1})^2 \tilde{\mu}_{\rm crit}}{m_G^2} \exp\left(-{\rm const}\frac{\tilde{\mu}_{\rm crit}^2}{m_G^2}\right), \tag{5.20}$$

where we assumed that $\Delta m \ll m$. Here we see again that $\Delta m_{\rm crit}$ monotonically decreases as $\tilde{\mu}_{\rm crit}$ becomes larger.

VI. COMMENTS ON 2D-4D CORRESPONDENCE

A. Brane picture and 2d-4d matching conditions

So far we have considered the μ-deformed 2d $CP(N-1)$ model *per se*, which is self-consistent. Let us now briefly comment on the requirements for the self-consistent treatment of this 2d theory considered as the world sheet theory of the non-Abelian string in $\mathcal{N}=2$ supersymmetric QCD, deformed by a mass term μ for the adjoint matter. At $\mu = 0$ the 2d-4d correspondence is seen from a different perspective. At the quantum level the situation is rather subtle since the 4d instantons interfere with the 2d world sheet theory, which makes the problem quite nontrivial. Fortunately it has been shown that 2d-4d correspondence is seen in the matching of renormalization group flows of 2d and 4d coupling constants, the coincidence of the spectra of Bogomol'nyi-Prasad-Sommereld (BPS) states [3,4,31], and the conformal dimensions at Argyres-Douglas critical points [32]. A general discussion concerning the decoupling limits when the 4d d.o.f. do not influence the world sheet theory can be found in [33].

In the brane engineering of $\mathcal{N}=2$ supersymmetric QCD the matching is nothing but the claim that one and the same object cannot change if we look at it as 4d or 2d observers. The standard IIA picture involves two parallel NS5 branes, N parallel D4 branes stretched between them, and N_f flavor branes which can be realized as semi-infinite D4' branes or equivalently as Kaluza-Klein (KK) monopoles [34]. When lifted to the M-theory the whole configuration gets identified as the single M5 brane wrapped around the Seiberg-Witten curve in the KK monopole background. The non-Abelian string is represented by the D2 brane stretched between two NS5 branes along some internal coordinate, say x_7. Its length in this direction δx_7 coincides with the 4d Fayet-Iliopoulos (FI) term and yields the tension of the dynamical non-Abelian string. The 4-4 strings yield the 4d gauge bosons, the 4-4' strings yield the chiral fundamental multiplets, while 2-4' strings yield the hypers in 2d theory. The 4d gauge coupling constant gets identified with the distance between NS5 branes $\delta x_6 \propto \frac{1}{g_{4d}^2}$ and exactly the same geometric variable coincides with the FI term in 2d theory. That is why the β functions in 4d and 2d theories coincide and geometrically reflect the backreaction of D4 and D4' branes on NS5 branes. The matching of the spectrum of BPS states in 4d and 2d theories has the geometrical origin as well. The BPS dyons are represented as properly embedded into the brane geometry D2 branes which geometrically are seen as the dyonic kinks on the world sheet of the non-Abelian string.

If we switch on the μ deformation, one of the NS5 branes world sheet gets rotated. Now the M5 brane is wrapped around holomorphic curve $w = W'(v)$ in (v, w, t) space where $x_4 + ix_5 = v$, $x_8 + ix_9 = w$, $x_6 + ix_{10} = t$, and W is the superpotential of the 4d theory. The embedding of the D2 or M2 brane representing the non-Abelian string has been discussed in [35]. It was argued that the M2 brane stretched between two M5 branes has a single possible stable embedding which fits with the single vacuum in 2d theory.

In this paper we consider a bit different solution when the tension of the string is fixed not by the FI term but by the mass of adjoint $T \propto \mu m$. This means that there is no immediate identification of the string tension with the distance between NS branes, and therefore the 4d and 2d couplings cannot be immediately identified in the brane geometry as it was done in the $\mathcal{N}=2$ case. As expected from the brane picture the β functions in 4d and 2d theories indeed are not identical now and the nonperturbative scales are related in a complicated manner [16]. It is better to use in this case the IIB picture where the non-Abelian string is represented by a D3 brane with world volume coordinates (x, t, D) where D is the disk in the internal space whose area yields the tension of the string.

One more input from the brane picture can be recognized if we look more carefully at the background where the probe M2 brane is placed. Apart from the M5 boundary conditions at the ends the background involves the N_f KK monopoles in M theory. Asymptotically the geometry involves the factors C^2/Z_{N_F} due to the Taub-NUT metric induced by flavor branes. Fortunately we can use some results concerning M2 probes in geometry involving Taub-NUT factors [36]. The terms of interest are the Chern-Simons terms with opposite levels for $U(N)_k \times U(N)_{-k}$ for N M2 branes. In our case we have the $U(1) \times U(1)$ gauge group for the nondynamical gauge field. As was argued in [36] a kind of Higgs mechanism works and only the diagonal $U(1)$ survives. What is the remnant of the 3d Chern-Simons

[5]In the numerical calculations for this paper, we took $N = 16$. a rough estimate of the accuracy from (5.17) and (5.18) is $1 - N^{-1/(N-1)} \approx 0.17$; i.e., qualitatively we can trust our results.

(CS) terms in the 2d world sheet theory? We can define the field $a(x)$ as

$$\exp(ia(x)) = \exp \int A_z(x,z)dz, \tag{6.1}$$

where z is the compact world volume coordinate of the M2 brane. The 3d CS term induces the axion on the string world sheet

$$\delta L = N_f \int d^2x a(x) * F. \tag{6.2}$$

Note that the CS term on the M2 brane emerges as a result of the one-loop integration over the world sheet fermions which do not decouple completely; therefore it cannot be seen in the classical approximation. If we consider the representation of the non-Abelian string via the D3 brane in IIB string theory, the effective axion on the world sheet emerges as well in a similar manner. However, the possible appearance of the effective axion in 2d theory should be clarified accurately. We cannot exclude that the CS and axion term disappear in the limit of complete decoupling of 4d d.o.f.

B. Bulk criticality and world sheet theory

One could question if the bulk criticality can be recognized in the world sheet theory. Consider the first large N limit of $\mathcal{N} = 2$ supersymmetric QCD with $N = N_f$ and assume that all quark masses are equal. It was shown in [37] making use of the exact Seiberg-Witten solution that there is a second order phase transition at $m = 2\Lambda$. In particular, it was shown that there is a jump of the derivative of the prepotential at this point. We could question if there are traces of this bulk phase transition in our string world sheet theory at $\Delta m = 0$. In $\mathcal{N} = 2$ theory the 4d-2d duality works well; hence the phase transition in the world sheet could be expected indeed. However, in the $\mathcal{N} = 2$ limit of our U(N) SQCD the average quark mass can be shifted away; therefore we cannot compare our results with that of Ref. [37]. The only hope is that we can identify remnants of this phase transition at nonzero μ. The 4d phase transition cannot disappear if we switch on small parameter μ; however, in order to consider strings semiclassically we restrict ourselves to the weak coupling regime in 4d theory which implies that the parameter which fixes the string tension $\xi \propto \mu m$ is large. Therefore at small μ we are forced to assume very large m and the phase transition point $m = 2\Lambda$ is far beyond our approximation. Nevertheless it would be very interesting to investigate the fate of the phase transition found in [37] at large μ.

One more example of bulk criticality occurs if the average mass m is very large but $\Delta m \propto \Lambda$. This is an example of the 4d Argyres-Douglas (AD) point when the theory becomes superconformal. It was shown in [32] that 4d and 2d AD points match perfectly and there is a matching of the critical exponents as well. Our critical point at $\mu = 0$ separating strong coupling and Higgs phases matches with a point $\Delta m = \Lambda$ on the curve (wall) of marginal stability. This curve forms a circle $|\Delta m| = \Lambda$ in the large N limit [38], and the 2d AD point is a point on this circle with a nonzero phase. If we switch on μ we expect that the 2d AD point survives and at small μ evolves smoothly. The clear-cut example of such smooth interpolation of the AD point has been elaborated for μ-deformed $SU(2)$ gauge group with $N_f = 1$ in [39] where it was identified as the deconfinement phase transition.

The final remark concerns the holographic picture which is possible since we consider the large N SQCD in the Veneziano limit. Instead of the D3 brane in the background of NS5 and D5 branes in IIB supergravity holographically we consider the D3 brane in peculiar 10d geometry with additional dilaton and form fields. The corresponding geometry has been identified for a pure $\mathcal{N} = 1$ limit at $\mu \to \infty$ in [40,41] and, in particular, it reproduces the correct Novikov-Shifman-Vainshtein-Zakharov beta function. For the generic μ the exact metrics is unknown but we expect that the mass term amounts to the effective wall at the corresponding value of the radial coordinate. A very illuminating example of how the bulk phase transition is seen on the probe string in the holographic framework has been found in [42] for $\mathcal{N} = 2^*$ theory. In this case the exact holographic background is known and coincides with the Pilch-Warner solution in IIB supergravity. The bulk theory enjoys the phase transition at strong coupling at the mass of adjoint $M = \Lambda$. It turns out that this phase transition indeed can be identified as criticality in the world sheet theory of electric probe string at the second order in the perturbation theory in the inverse t'Hooft coupling at strong coupling. This clearly demonstrates that the 2d-4d matching of bulk and world sheet criticality is highly nontrivial in the holographic picture. It would be interesting to investigate the non-Abelian magnetic string in the background found in [40,41].

VII. CONCLUSIONS: PHASE DIAGRAM

In this paper we have studied dynamics of the μ-deformed $CP(N-1)$ model (2.13). It arises as a world sheet theory of the non-Abelian string in $\mathcal{N} = 2$ supersymmetric QCD, deformed by a mass term μ for the adjoint matter. When $\tilde{\mu}$ is small, the two-dimensional theory is the $\mathcal{N} = (2,2)$ supersymmetric $CP(N-1)$ model. As we increase the deformation parameter, the bulk theory flows to $\mathcal{N} = 1$ SQCD, while the world sheet theory becomes a nonsupersymmetric μ-deformed $CP(N-1)$ model. This happens because fermion zero modes present in the bulk of the $\mathcal{N} = 2$ theory are lifted when we switch on $\tilde{\mu}$. As a consequence, at large $\tilde{\mu}$ world sheet fermions become heavy and decouple, leaving us with the pure bosonic $CP(N-1)$ model. In this paper we studied this transition in detail using the large N approximation.

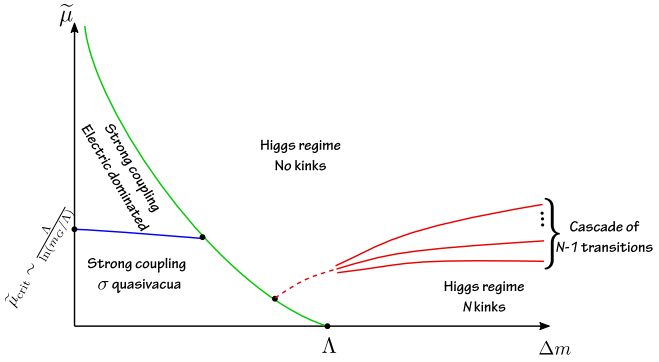

FIG. 15. Whole phase diagram (schematically). Δm on the horizontal axis, and $\tilde{\mu}$ on the vertical axis. The cascade of $N-1$ curves corresponds to the disappearance of kinks between the ground state and quasivacua. Dashed lines are drawn based on a general argument, since the $1/N$ expansion gives a poor approximation in this region.

The μ-deformed $CP(N-1)$ model has two N-independent parameters, the deformation $\tilde{\mu}$ [see (2.18)] and the mass scale Δm which is the scale of the quark mass differences in the bulk theory. We obtained a nontrivial phase diagram in the $(\Delta m, \tilde{\mu})$ plane, with two strong coupling phases and two Higgs phases separated by three critical curves with two tricritical points. This phase diagram is shown in Fig. 15.

When $\tilde{\mu}$ goes to zero, the supersymmetry is unbroken, and the theory is either in the strong coupling phase (at small Δm) or in the Higgs phase (large Δm, weak coupling). In both phases there are N degenerate vacua, and kinks interpolating between neighboring vacua are not confined. In the strong coupling phase at small Δm the photon becomes dynamical and acquires mass due to the chiral anomaly.

As we switch on the deformation parameter degenerate vacua split. At strong coupling we get a unique ground state and $N-1$ quasivacua, while the photon develops a small massless component. Kinks are now confined. When the deformation $\tilde{\mu}$ is small, the confinement is due to the splitting of the σ-quasivacua energies. As $\tilde{\mu}$ gets larger, eventually we cross the critical line where original σ quasivacua decay. Now the quasivacua splitting and confinement of kinks is only due to the constant electric field.

In the Higgs phase at large Δm the theory is at weak coupling. The n field develops a VEV, and the photon is unphysical and heavy due to the Higgs mechanism. When $\tilde{\mu}$ is small enough, energies of N degenerate vacua split, and kinks interpolating between the neighboring quasivacua are confined. However, as we increase $\tilde{\mu}$, it crosses critical lines where [see, e.g., (5.9)] quasivacua decay one by one leaving the theory with a single ground state, and thus without kinks.

In this paper we have shown that results obtained in [16] for the μ-deformed bulk theory agree with the world sheet considerations. We can either go to the world sheet in the $\mathcal{N}=2$ theory and then take the large $\tilde{\mu}$ limit or first apply the large deformation in the bulk and then go to the world sheet theory. In other words, the following diagram is commutative:

$$\begin{array}{ccc} 4\text{d } \mathcal{N}=2 \text{ SQCD} & \xrightarrow[\text{worldsheet}]{} & 2\text{d } \mathcal{N}=(2,2)\ CP(N-1) \\ \text{large } \tilde{\mu} \downarrow & & \text{large } \tilde{\mu} \downarrow \\ 4\text{d } \mathcal{N}=1 \text{ SQCD} & \xrightarrow[\text{worldsheet}]{} & 2\text{d } \mathcal{N}=0\ CP(N-1) \end{array} \tag{7.1}$$

We note, however, that a derivation of the world sheet theory at intermediate values of $\tilde{\mu}$ is still absent.

As we already discussed we interpret kinks of the world sheet theory as confined monopoles of the four-dimensional SQCD. Our results show, in particular, that at large $\tilde{\mu}$, when the bulk theory basically becomes $\mathcal{N}=1$ SQCD, monopoles survive only in the strong coupling phase at very small mass differences below the critical line (5.20). In the Higgs phase quasivacua decay at large $\tilde{\mu}$ which means that confined monopole and antimonopole forming a "meson" on the string (see Fig. 1) annihilate each other and disappear. This confirms a similar conclusion in [16].

ACKNOWLEDGMENTS

The authors are grateful to M. Shifman for valuable discussions. The work of A. G. was supported in part by Basis Foundation fellowship and RFBR Grant No. 19-02-00214. A. G. thanks FTPI at University of Minnesota, Simons Center for Geometry and Physics at Stony Brook University, and Kavli Institute at UCSB where parts of the work has been done for the hospitality and support. The part of work of E. I. concerning the calculation of the diagrams and the strong coupling effective action was funded by Russian Foundation for Basic Research (RFBR) according to the research Projects No. 18-32-00015 and No. 18-02-00048, and the rest of his work by the Foundation for the Advancement of Theoretical Physics and Mathematics "BASIS" according to the research Project No. 19-1-5-106-1. The work of A. Y. was supported by William I. Fine Theoretical Physics Institute, University of Minnesota, Skolkovo Institute of Science and Technology and by Russian Foundation for Basic Research Grant No. 18-02-00048.

APPENDIX A: COEFFICIENTS OF THE EFFECTIVE ACTION

In this appendix we give a brief overview of the derivation of the effective action (4.23). Consider bosonic loops. In the Lagrangian (2.13) we can expand the $\sigma - n$ interaction term as

$$\begin{aligned}&|\sqrt{2}\sigma - m_i|^2|n^i|^2\\ &\approx |\sqrt{2}\langle\sigma\rangle - m_i|^2|n^i|^2 + 2\Re(\sqrt{2}\delta\sigma)\cdot(\sqrt{2}\langle\sigma\rangle - \Re m_i)|n^i|^2\\ &\quad - 2\Im(\sqrt{2}\delta\sigma)\cdot\Im m_i|n^i|^2,\end{aligned} \tag{A1}$$

where $\delta\sigma$ are the vacuum fluctuations around the vacuum with $\Im\sigma = 0$. The diagram for the $\Re\sigma$ kinetic term is then proportional to $(\sqrt{2}\langle\sigma\rangle - \Re m_i)^2$, while the kinetic term for $\Im\sigma$ is proportional to $(\Im m_i)^2$. The calculation of the diagrams itself is straightforward.

The calculation of the fermion loops is a bit trickier. The fermion mass matrix can be read off from (2.13). Say, for the flavor number i,

$$M_i = (\sqrt{2}\langle\sigma\rangle - \Re m_i)\cdot \mathrm{Id} + i(\Im m_i)\cdot\gamma_{\mathrm{chir}}, \tag{A2}$$

where Id is the 2×2 identity matrix and γ_{chir} is the two-dimensional analogue of the γ_5. This γ_{chir} interferes with the traces over the spinorial indices. Say, the fermionic contribution to the $\Re\sigma$ kinetic term coming from the diagram on Fig. 4(b) is

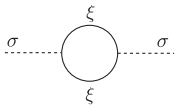

$$\begin{aligned}&= -(i\sqrt{2})^2\sum_i\int\frac{d^2k}{(2\pi)^2}\mathrm{Tr}\left[\frac{i}{\not k - M_i}\frac{i}{\not k + \not q - M_i}\right]\\ &= -2\sum_i\int\frac{d^2k}{(2\pi)^2}\mathrm{Tr}\left[\frac{\not k + M_i^\dagger}{k^2 - |M_i|^2}\frac{\not k + \not q + M_i^\dagger}{(k+q)^2 - |M_i|^2}\right]\\ &= -4\sum_i\int\frac{d^2k}{(2\pi)^2}\mathrm{Tr}\left[\frac{(k\cdot(k+q)) + \left(\sqrt{2}\langle\sigma\rangle - \Re m_i\right)^2 - (\Im m_i)^2}{(k^2 - |M_i|^2)((k+q)^2 - |M_i|^2)}\right]\end{aligned} \tag{A3}$$

where $|M_i|^2 = (\sqrt{2}\langle\sigma\rangle - \Re m_i)^2 + (\Im m_i)^2$. Calculation of the integral itself is straightforward. The rest of the diagrams with fermionic loops are treated the same way. In the end we arrive at (4.25).

Note that in the limit $\tilde\mu \to 0$ supersymmetry is restored. In this case, in the vacuum $D = 0$, $\Im\sigma = 0$ we have

$$M^2_{\xi_k} = m^2_{n_k} = |\sqrt{2}\langle\sigma\rangle - m_k|^2, \tag{A4}$$

and the coefficients (4.25) reduce to

$$\frac{1}{e^2_{\Re\sigma}} = \frac{1}{e^2_{\Im\sigma}} = \frac{1}{e^2_\gamma} = \frac{1}{4\pi}\sum_{k=0}^{N-1}\frac{1}{|\sqrt{2}\langle\sigma\rangle - m_k|^2}, \tag{A5}$$

$$b_{\gamma,\Im\sigma} = \frac{1}{2\pi}\sum_{k=0}^{N-1}\frac{1}{\sqrt{2}\langle\sigma\rangle - m_k}. \tag{A6}$$

APPENDIX B: PHOTON MASS

In this appendix we diagonalize the photon-σ mass matrix in (4.23) to find the photon mass. In order to do that, let us write down bare propagators for $\Im\sigma$ and A_μ that follow immediately from (4.23) (in the Minkowski notation):

$$G^0_\gamma = -ie^2_\gamma\frac{g^{\mu\nu} - \frac{k^\mu k^\nu}{k^2}}{k^2}, G^0_{\Im\sigma} = -\frac{i}{2}e^2_{\Im\sigma}\frac{1}{k^2 - \delta m^2_{\Im\sigma}}, \tag{B1}$$

where we use the Landay gauge, while $\delta m^2_{\Im\sigma}$ is the contribution to the mass of the $\Im\sigma$ field coming from the potential $V(\sigma)$ in (4.23). In the vicinity of the true ground state (4.17) we have

$$\delta m^2_{\Im\sigma} \approx 4\lambda\Lambda\ln\frac{m_G}{\Lambda}. \tag{B2}$$

At large $\tilde\mu$, $\delta m^2_{\Im\sigma} \sim \lambda^2\ln m_G/\Lambda$; see Sec. IV D.

Consider the photon propagator. Iterating the scalar $\Im\sigma$ insertions shown in Fig. 16, we obtain the full photon propagator,

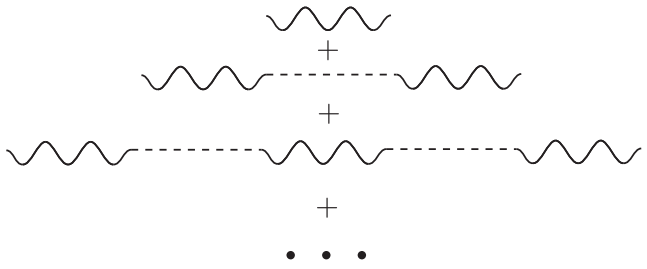

FIG. 16. Contributions to the photon propagator.

$$\hat{G}_\gamma = G^0_\gamma \frac{1}{1-\frac{e^2_\gamma e^2_{\Im\sigma} b^2_{\gamma,\Im\sigma}}{k^2-\delta m^2_{\Im\sigma}}} = -ie^2_\gamma\left(g^{\mu\nu}-\frac{k^\mu k^\nu}{k^2}\right)\frac{k^2-\delta m^2_{\Im\sigma}}{k^2(k^2-\delta m^2_{\Im\sigma}-e^2_\gamma e^2_{\Im\sigma} b^2_{\gamma,\Im\sigma})} = -ie^2_\gamma\left(g^{\mu\nu}-\frac{k^\mu k^\nu}{k^2}\right)\left(A\frac{1}{k^2}+(1-A)\times\frac{1}{k^2-\delta m^2_{\Im\sigma}-e^2_\gamma e^2_{\Im\sigma} b^2_{\gamma,\Im\sigma}}\right), \tag{B3}$$

where the coefficient

$$A = \frac{\delta m^2_{\Im\sigma}}{\delta m^2_{\Im\sigma} + e^2_\gamma e^2_{\Im\sigma} b^2_{\gamma,\Im\sigma}} \tag{B4}$$

increases from 0 to 1 as $\tilde{\mu}$ runs from zero to infinity. What we see here is that at nonzero $\tilde{\mu}$, the photon acquires a massless component. In the SUSY case (zero $\tilde{\mu}$) the coefficient A vanishes, and we have only the massive component. Note that the number of physical states do not change since the massless photon has no physical d.o.f. in two dimensions. At large $\tilde{\mu}$ the massive component becomes heavy and decouples ($A \to 1$). We are left with the massless photon much in the same way as in the nonsupersymmetric $CP(N-1)$ model.

If we do a similar calculation for the $\Im\sigma$ propagator, we will get simply

$$\hat{G}_{\Im\sigma} = G^0_{\Im\sigma}\frac{1}{1-\frac{e^2_\gamma e^2_{\Im\sigma} b^2_{\gamma,\Im\sigma}}{k^2-\delta m^2_{\Im\sigma}}} = -ie^2_{\Im\sigma}\frac{1}{k^2-\delta m^2_{\Im\sigma}-e^2_\gamma e^2_{\Im\sigma} b^2_{\gamma,\Im\sigma}}. \tag{B5}$$

Just as in [18], we see that the would-be massless phase of the σ field acquires a mass

$$m^2_{\arg\,\tau} = \delta m^2_{\Im\sigma} + e^2_\gamma e^2_{\Im\sigma} b^2_{\gamma,\Im\sigma}. \tag{B6}$$

This effect is taken into account by the additional term (4.5) in the effective potential (4.3). At $\tilde{\mu}=0$, $\delta m^2_{\Im\sigma}=0$ and the mass of the phase of σ reduces to (4.6). Consider the leading correction at small λ. For the ground state (4.17) at $\Delta m = 0$ we have

$$\frac{1}{e^2_{\Im\sigma}} \approx \frac{N}{4\pi\Lambda^2}\left(1-2\frac{\lambda}{\Lambda}\ln\frac{m_G}{\Lambda}\right),\quad \frac{1}{e^2_\gamma} \approx \frac{N}{4\pi\Lambda^2}\left(1-\frac{4}{3}\frac{\lambda}{\Lambda}\ln\frac{m_G}{\Lambda}\right),\quad b_{\gamma,\Im\sigma} \approx -\frac{N}{2\pi\Lambda}\left(1-\frac{\lambda}{\Lambda}\ln\frac{m_G}{\Lambda}\right),$$

and, therefore,

$$m^2_{\arg\,\tau} \approx 4\Lambda^2\left(1+\frac{7}{3}\frac{\lambda}{\Lambda}\ln\frac{m_G}{\Lambda}\right). \tag{B7}$$

Let us look more closely at the photon propagator (B3) in the small $\tilde{\mu}$ limit. We have

$$A \approx \frac{\lambda}{\Lambda}\ln\frac{M}{\Lambda}, \tag{B8}$$

and for the massless part of the photon propagator,

$$\hat{G}_{\gamma,\text{massless}} = -i\frac{g^{\mu\nu}-\frac{k^\mu k^\nu}{k^2}}{k^2}\frac{4\pi}{N}\lambda\Lambda\ln\frac{M}{\Lambda}. \tag{B9}$$

From this Green function we calculate the electric field produced by a kink with electric charge $+1$ and find for the vacuum energy splitting

$$E_1 - E_0 = \frac{1}{2e^2_\gamma}F^2_{01} = \frac{2\pi}{N}\left(\lambda\ln\frac{M}{\Lambda}\right)^2. \tag{B10}$$

[1] A. Hanany and D. Tong, Vortices, instantons and branes, J. High Energy Phys. 07 (2003) 037.
[2] R. Auzzi, S. Bolognesi, J. Evslin, K. Konishi, and A. Yung, Non-Abelian superconductors: Vortices and confinement in $\mathcal{N}=2$ SQCD, Nucl. Phys. **B673**, 187 (2003).
[3] M. Shifman and A. Yung, Non-Abelian string junctions as confined monopoles, Phys. Rev. D **70**, 045004 (2004).
[4] A. Hanany and D. Tong, Vortex strings and four-dimensional gauge dynamics, J. High Energy Phys. 04 (2004) 066.
[5] D. Tong, TASI Lectures on Solitons: Instantons, monopoles, vortices and kinks, arXiv:hep-th/0509216.
[6] M. Eto, Y. Isozumi, M. Nitta, K. Ohashi, and N. Sakai, Solitons in the Higgs phase: The moduli matrix approach, J. Phys. A **39**, R315 (2006).
[7] M. Shifman and A. Yung, Supersymmetric solitons, Rev. Mod. Phys. **79**, 1139 (2007); an expanded version in Cambridge University Press, 2009.
[8] D. Tong, Quantum vortex strings: A review, Ann. Phys. (Amsterdam) **324**, 30 (2009).
[9] M. Shifman and A. Yung, Lessons from supersymmetry: "Instead-of-Confinement" mechanism, Int. J. Mod. Phys. A **29**, 1430064 (2014).

[10] N. Seiberg and E. Witten, Electric-magnetic duality, monopole condensation, and confinement in N = 2 supersymmetric Yang-Mills theory, Nucl. Phys. **B426**, 19 (1994); Erratum, Nucl. Phys. **B430**, 485 (1994).
[11] N. Seiberg and E. Witten, Monopoles, duality and chiral symmetry breaking in N = 2 supersymmetric QCD, Nucl. Phys. **B431**, 484 (1994).
[12] A. Abrikosov, Zh. Eksp. Teor. Fiz. **32**, 1442 (1957) [On the magnetic properties of superconductors of the second group, Sov. Phys. JETP **5**, 1174 (1957)]; H. Nielsen and P. Olesen, Vortex-line models for dual strings, Nucl. Phys. **B61**, 45 (1973); Reprinted in *Solitons and Particles*, edited by C. Rebbi and G. Soliani (World Scientific, Singapore, 1984), p. 365.
[13] M. Shifman and A. Yung, Non-Abelian flux tubes in N = 1 SQCD: Supersizing world-sheet supersymmetry, Phys. Rev. D **72**, 085017 (2005).
[14] M. Edalati and D. Tong, Heterotic vortex strings, J. High Energy Phys. 05 (2007) 005.
[15] M. Shifman and A. Yung, Heterotic flux tubes in $\mathcal{N} = 2$ SQCD with $\mathcal{N} = 1$ preserving deformations, Phys. Rev. D **77**, 125016 (2008); Errarum, Phys. Rev. D **79**, 049901 (2009).
[16] E. Ievlev and A. Yung, Non-Abelian strings in $\mathcal{N} = 1$ supersymmetric QCD, Phys. Rev. D **95**, 125004 (2017).
[17] D. Tong, Monopoles in the Higgs phase, Phys. Rev. D **69**, 065003 (2004).
[18] E. Witten, Instantons, the quark model, and the 1/N expansion, Nucl. Phys. **B149**, 285 (1979).
[19] A. Gorsky, M. Shifman, and A. Yung, Non-Abelian Meissner effect in Yang-Mills theories at weak coupling, Phys. Rev. D **71**, 045010 (2005).
[20] E. Witten, Phases of N = 2 theories in two dimensions, Nucl. Phys. **B403**, 159 (1993).
[21] A. Gorsky, M. Shifman, and A. Yung, The Higgs and Coulomb/confining phases in 'twisted-mass' deformed CP(N-1) model, Phys. Rev. D **73**, 065011 (2006).
[22] P. A. Bolokhov, M. Shifman, and A. Yung, Heterotic N = (0, 2) CP(N-1) model with twisted masses, Phys. Rev. D **81**, 065025 (2010).
[23] V. Markov, A. Marshakov, and A. Yung, Non-Abelian vortices in N = 1^* gauge theory, Nucl. Phys. **B709**, 267 (2005).
[24] F. Ferrari, Large N and double scaling limits in two dimensions, J. High Energy Phys. 05 (2002) 044.
[25] F. Ferrari, Non-supersymmetric cousins of supersymmetric gauge theories: Quantum space of parameters and double scaling limits, Phys. Lett. B **496**, 212 (2000); A model for gauge theories with Higgs fields, J. High Energy Phys. 06 (2001) 057.
[26] P. A. Bolokhov, M. Shifman, and A. Yung, Large-N solution of the heterotic $CP(N-1)$ model with twisted masses, Phys. Rev. D **82**, 025011 (2010); Erratum, Phys. Rev. D **89**, 029904 (2014).
[27] M. Shifman and A. Yung, Moduli space potentials for heterotic non-Abelian flux tubes: Weak deformation, Phys. Rev. D **82**, 066006 (2010).
[28] M. Shifman and A. Yung, Large-N solution of the heterotic N = (0, 2) two-dimensional CP(N-1) model, Phys. Rev. D **77**, 125017 (2008); Erratum, Phys. Rev. D **81**, 089906 (2010).
[29] V. Novikov, M. Shifman, A. Vainshtein, and V. Zakharov, Two-dimensional sigma models: Modelling non-perturbative effects in quantum chromodynamics, Phys. Rep. **116**, 103 (1984).
[30] T. Appelquist and J. Carazzone, Infrared singularities and massive fields, Phys. Rev. D **11**, 2856 (1975).
[31] N. Dorey, The BPS spectra of two-dimensional supersymmetric gauge theories with twisted mass terms, J. High Energy Phys. 11 (1998) 005; N. Dorey, T. J. Hollowood, and D. Tong, The BPS spectra of gauge theories in two-dimensions and four-dimensions, J. High Energy Phys. 05 (1999) 006.
[32] D. Tong, Superconformal vortex strings, J. High Energy Phys. 12 (2006) 051.
[33] K. Hori, C. Y. Park, and Y. Tachikawa, 2d SCFTs from M2-branes, J. High Energy Phys. 11 (2013) 147.
[34] E. Witten, Solutions of four-dimensional field theories via M theory, Nucl. Phys. **B500**, 3 (1997).
[35] D. Gaiotto, S. Gukov, and N. Seiberg, Surface defects and resolvents, J. High Energy Phys. 09 (2013) 070.
[36] O. Aharony, O. Bergman, D. L. Jafferis, and J. Maldacena, $N = 6$ superconformal Chern-Simons-matter theories, M2-branes and their gravity duals, J. High Energy Phys. 10 (2008) 091.
[37] J. G. Russo and K. Zarembo, Massive $N = 2$ gauge theories at large N, J. High Energy Phys. 11 (2013) 130.
[38] S. Olmez and M. Shifman, Curves of marginal stability in two-dimensional CP(N-1) models with Z(N)-symmetric twisted masses, J. Phys. A **40**, 11151 (2007).
[39] A. Gorsky, A. I. Vainshtein, and A. Yung, Deconfinement at the Argyres-Douglas point in $SU(2)$ gauge theory with broken $N = 2$ supersymmetry, Nucl. Phys. **B584**, 197 (2000).
[40] A. Barranco, E. Pallante, and J. G. Russo, $N = 1$ SQCD-like theories with N_f massive flavors from AdS/CFT and beta functions, J. High Energy Phys. 09 (2011) 086.
[41] R. Casero, C. Nunez, and A. Paredes, Elaborations on the string dual to N = 1 SQCD, Phys. Rev. D **77**, 046003 (2008).
[42] J. G. Russo, E. Widn, and K. Zarembo, $N = 2^*$ phase transitions and holography, J. High Energy Phys. 02 (2019) 196.